Introduction to photochemical processes for environmental purposes

The case of vanadium-based oxides

Olivier Monfort

Comenius University Bratislava

Comenius University Bratislava
Faculty of Natural Sciences

Olivier Monfort

Introduction to photochemical processes for environmental purposes

The case of vanadium-based oxides

2022

Comenius University Bratislava

Department of Inorganic Chemistry, Faculty of Natural Sciences, Comenius University Bratislava

Reviewers: Prof. Dr. Marcello Brigante, Université Clermont Auvergne, France
Ing. Marcel Šihor, Ph.D., MBA, MSc., VŠB – Technical University of Ostrava, Czech republic

Edited by author.

77 pages, 4,69 author's sheets, first edition, released as an electronic publication.

Comenius University Bratislava

ISBN 978-80-223-5380-9

Table of Contents

Introduction

This university textbook is focused on inorganic chemistry and more particularly on materials chemistry, photochemistry and environmental chemistry. Therefore, it is intended for a student audience specialized in the field of chemistry. This university textbook can be used for the following subjects in MSc. and PhD. programmes in Inorganic Chemistry:

Advanced Inorganic Chemistry I and II – PhD. programme

Materials chemistry – MSc. programme

Photochemical processes – MSc. programme

Nanostructured substances in materials chemistry – MSc. programme

Environmental applications of inorganic substances – MSc. programme

This pedagogical work is focused on vanadium-based oxides which are promising materials that can be used in photochemical processes for environmental purposes including the degradation of organic pollutants and the production of hydrogen by water splitting. The preparation procedure of these oxides is crucial to design the appropriate phase, crystal structure, morphology, electronic band structure, etc. that govern the physico-chemical properties of the final material. Vanadium-based oxides can be used as solar light-driven photocatalysts for the treatment of water since reactive oxygen species ($HO^{\bullet}$, $O_2^{\bullet -}$, etc.) can be generated. In addition, some of these oxides have an appropriate electronic band structure to split water molecule into hydrogen which is considered as green fuel. Such environmental problematics are crucial for the current and next generations. This university textbook provides the basic knowledge and a comprehensive overview of the use of photochemical processes for environmental purposes using vanadium-based oxides.

Úvod

Tieto vysokoškolské skriptá sú zamerané na anorganickú chémiu, konkrétne na materiálovú chémiu, fotochémiu a chémiu životného prostredia. Sú určené pre študentov špecializujúcich sa na oblasť chémie. Skriptá možno použiť ako študijný materiál v magisterskom i PhD. stupni štúdia anorganickej chémie v rámci nasledujúcich predmetov:

Pokročilá anorganická chémia I a II – PhD. program,

Chémia materiálov – magisterský program,

Fotochemické procesy – magisterský program,

Nanoštruktúrne látky v materiálovej chémii – magisterský program,

Environmentálne aplikácie anorganických látok – magisterský program.

Táto pedagogická práca je zameraná na oxidy na báze vanádu, ktoré patria medzi perspektívne materiály využiteľné vo fotochemických procesoch na environmentálne účely vrátane degradácie organických polutantov a produkcie vodíka štiepením vody. Postup prípravy týchto oxidov je rozhodujúci na dosiahnutie vhodnej fázy, kryštálovej štruktúry, morfológie, štruktúry elektronického pásu a pod., ktoré určujú fyzikálno-chemické vlastnosti konečného materiálu. Oxidy na báze vanádu možno použiť ako fotoaktalyzátory poháňané slnečným svetlom na úpravu vody vďaka tvorbe reaktívnych foriem kyslíka ($HO^{\bullet}$, $O_2^{\bullet-}$ a pod.). Navyše niektoré z týchto oxidov majú vhodnú štruktúru elektronického pásu na štiepenie molekúl vody na vodík, ktorý sa považuje za tzv. zelené palivo. Prezentované environmentálne problémy sú kľučové pre súčasnú a budúcu generáciu. Tieto vysokoškolské skriptá poskytujú základné poznatky a ucelený prehľad o využití fotochemických procesov na environmentálne účely s použitím oxidov na báze vanádu.

List of abbreviation

AOP: Advanced Oxidation Process

CB: Conduction Band

CBM: Conduction Band Minimum

CEC: Contaminants of Emerging Concern

DFT: Density Functional Theory

DMPO: 5,5-dimethyl-1-pyrroline N-oxide

DNA: Deoxyribonucleic acid

e^-: photogenerated electron

EDC: Endocrine Disruptor Compound

E_g: Energy Bandgap

EPR: Electron Paramagnetic Resonance

h^+: photogenerated hole

IPCE: Incident Photon-to-Current Efficiency

IR: Infrared

LIB: Lithium-Ions Battery

LMCT: Ligand-to-Metal Charge Transfer

MIT: Metal-to-Insulator Transition

PEC: Photoelectrochemical

POP: Persistent Organic Pollutant

PPCP: Pharmaceutical and Personal Care Products

ROS: Reactive Oxygen Species

SHE: Standard Hydrogen Electrode

SSA: Specific Surface Area

TAS: Transient Absorption Spectroscopy

T_c: Critical Temperature

TCR: Temperature Coefficient of Resistance

TMD: Transition Metal Dichalcogenide

US: United States

UV: Ultraviolet

VB: Valence Band

VBM: Valence Band Maximum

WWTP: Wastewater Treatment Plant

1 Context

1.1 Environmental context

The environmental remediation is one of the important challenges that the mankind is facing to. Indeed, the deterioration of the natural environment by contamination from anthropogenic activities is among the main issues the governments worldwide are fighting against. Recently, international agreements have been signed to limit the negative impacts of human activities on our planet such as, for instance, the Kyoto protocol in 1995, the Stockholm convention in 2001 and the Paris agreements in 2015. Beside these attempts, the development of sustainable technologies including the production of green energy and the treatment of the different environmental compartments (soil, water and air) is a requirement for the current and future generations.

Let's illustrate the environmental context with the example of water. The water resource is rare and precious: around 0.5% of water on the Earth is drinkable and accessible. In addition, this extremely small percentage is subjected to an imbalance between availability and demand which is caused by its overuse for domestic, industrial and agricultural purposes, but also by the climate disorder *i.e.* longer, more intense and more frequent droughts. Since the last industrial revolution, the water quality is being deteriorated due to anthropogenic activities, especially from factories in the field of textile, chemistry, agriculture, and pharmacy that are releasing into the natural environment their inefficiently treated wastewaters [1, 2, 3]. As a result, a lot of organic and inorganic contaminants such as pesticides and fertilizers, sulphur derivatives, active pharmaceutical ingredients, etc. can be find in the hydrosphere [1, 2, 3, 4]. Among them, many compounds are considered as persistent (persistent organic pollutants - POPs) or emerging (contaminants of emerging concern - CECs). For the latter category, their chemistry and interaction with the environment are unknown thus being potentially toxic for humans, animals and plants. It includes, for instance, endocrine disruptor compounds (EDCs) and pharmaceutical and personal care products (PPCPs) [5, 6, 7, 8]. Therefore, many national environmental agencies impose strict measures to limit such an environmental contamination [2]. However, limiting the pollution does not remediate the damages already caused to the planet, and the society should focus more on the development of sustainable technologies [9].

1.2 Photochemistry

Photochemistry is ubiquitous in the everyday life. The vision is based on a photochemical reaction with light-sensitive cell onto our retina, thus producing a signal which is transferred to our brain [1]. The coloration of our skin under the sun is also related to photochemistry where the melanin (a pigment) reacts under UV light, thus changing its colour. Also, the film photography is a technology based on photochemistry, especially on the reduction of Ag(I) into Ag^0 under flashlight. Concerning environmental photochemistry, the most known natural photochemical reaction is the photosynthesis. The photosynthesis, especially the oxygenic one, happens in organisms that contain chlorophyl which is a pigment where the process occurs. In the presence of carbon dioxide and water, organic matter (like carbohydrates) and oxygen can be produced under light. Another environmental photochemical process is above our heads: in the atmosphere, ozone (O_3) can be dissociated under UVB into oxygen (O_2) while the ionosphere is composed of O_2^+ and N_2^+ ions that are the result of reactions of N_2 and O_2 with light (from UVC to X-rays) [1]. This non-exhaustive list of concrete examples highlights the importance of photochemistry for the environment but also the life on Earth.

The photochemistry is defined as a branch of chemistry which is focused on the changes in chemical species brought by the absorption of light. The light as a wave is an electromagnetic radiation of any wavelength (IR, visible, UV, X-rays, etc.) while as a particle, it is defined as a photon which is a quantum of light corresponding to any electromagnetic radiation. Therefore, a photochemical reaction is a chemical reaction triggered by the absorption of photon. In photochemistry, it is important to distinguish 3 basics photophysical processes that occur when a molecule absorbs light: the light absorption causes the excitation of an electronic from fundamental singlet state to excited singlet state; the fluorescence corresponds to relaxation of an electron in an excited singlet state to a singlet state of lower energy, thus generating light emission; and the phosphorescence corresponds to relaxation of an electron in an excited triplet state (after internal conversion from excited singlet state) to a singlet state of lower energy, thus generating also light emission but lasting longer than in the fluorescence. In photochemistry, 2 important principles should be considered: the Gotthuss-Draper law (a photochemical reaction should involve a molecule that absorbs light)

and the Stark-Einstein law (one molecule can absorb only one photon). The photochemistry is a powerful tool that can be used for environmental purposes [2]. Indeed, many efforts have been devoted to the preparation of inorganic materials which have promising photochemical properties, especially for the remediation of the environment which is the main thematic developed in this monography.

2 Why vanadium?

2.1 Generalities

Vanadium is a transition metal (Group 5; Z = 23) with $3d^3 4s^2$ as valence electronic configuration [10]. It has a melting point at 1910 °C and presents different stable oxidation states from +II to +V [11]. Vanadium is discovered by Andres Manuel Del Rio in 1801 in the form of an ore, called today vanadinite ($Pb_5(VO_4)_3Cl$) [12, 13]. Vanadium was first named "panchromium" due to the wide variety of colours of its salts. In 1831, Nils Gabriel Sefstrom (re)discovered vanadium but in the form of an oxide and he named it after Vanadis, a goddess in the Nordic mythology [14]. In the earth's crust, vanadium is the 5th most abundant transition metal element (0.019%) and 22nd among all discovered elements [15, 16]. Vanadium can be found in various minerals like vanadinite, carnotite ($K_2(UO_2)_2(VO_4)_2 \cdot 3H_2O$), and patronite ($V(S_2)_2$) [13, 17].

Vanadium is a transition metal of high natural and biological importance since it is present in each environmental compartment and in living organisms, respectively. In sea water, vanadium is mainly in the form of $H_2VO_4^-$ and it is the 2nd most abundant transition metal element with a mean concentration of 2 $\mu g \cdot L^{-1}$ [13, 18]. The main natural sources for vanadium are marine aerosols, dust from soils and rocks weathering, and volcanic emissions [19, 20, 21, 22]. It can be also produced from anthropogenic activity, especially from mining and burning of fossil fuels. That is an issue since it results in atmospheric pollution with an estimation of more than 60 thousand tons each year with long period of residence time in the air [23, 24].

2.2 Biochemistry of vanadium

Vanadium is an essential biochemical element for several mammals, especially in some enzymes such as nitrogenase and haloperoxidase [13]. Vanadium in the form of vanadate (VO_4^{3-}) is isostructural to PO_4^{3-}, thus being a competitive compound with phosphate. Therefore, vanadate can inhibit several phosphate-metabolizing enzymes, and can lead to death at high levels [13, 25]. Indeed, vanadium becomes toxic to the human health during one-time exposure at value around 35 mg by inhalation [18, 26]. In the human body, vanadium enters in the blood through respiratory and gastro-intestinal systems (Figure 1) [27]. For example, vanadates ($H_2VO_4^-$) present in drinking water is partially reduced in the stomach before being precipitated in the intestines in the form of $VO(OH)_2$ [18]. Once in the blood, vanadium undergoes redox conversion between V(V) and V(IV) according to the level of oxygen and the presence of reductants/oxidants. Most of vanadium accumulates in vital organs such as kidneys, spleen and liver, and it is eliminated *via* urine or distributed in tissues (Figure 1) [28]. In the human body, the average vanadium concentration is approximatively 0.3 µM [29, 30, 31, 32, 33, 34, 35].

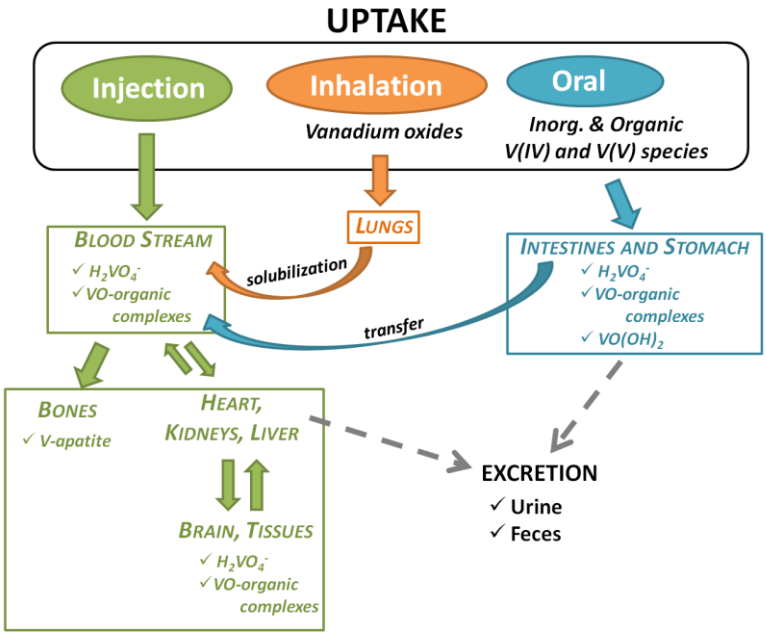

Figure 1. The pathway of vanadium in the human metabolism [36].

On the other hand, vanadium can be used in metallodrugs, especially for the treatment of diabetes. Indeed, the first use of vanadium in pharmacology was for this disease. Vanadium, in the form of salts (sodium metavanadate, sodium orthovanadate and vanadyl sulphate), can activate insulin receptor, thus triggering a positive effect on patients who need insulin. Vanadium is also used for the treatment of several pathologies such as obesity and hypertension, but also for anti-cancer treatments since it can protect the genomic stability by limiting the wear and tear of DNA [29, 37, 38]. As mentioned earlier, vanadate is isostructural to phosphate, thus inhibiting/activating several ATPases and phosphatases enzymes [29, 39].

2.3 Technologies using vanadium

Vanadium can be used in the form of materials in a wide range of technologies, especially in the form of chalcogenides *i.e.* oxides and sulphides, nitrides, carbides and halides [40]. The case of vanadium chalcogenides is developed in this section.

Vanadium sulphide (VS_2) has a structure composed of a vanadium layer which is sandwiched between two sulphide layers [41]. The VS_2 layers are stacked thank to Van der Walls bonding. VS_2 belongs to the class of transition metal dichalcogenide (TMD). Due to its layered structure and its excellent 2D conductivity, VS_2 can be used in energy storage devices and supercapacitors [42, 43, 44].

Vanadium oxides are more popular than sulphides. Some of these oxides are commercially available like, for instance, vanadium dioxide. Indeed, VO_2 as most of the vanadium oxides exhibit a metal-insulator transition (MIT) *i.e.* the properties of the oxide change reversible from insulating/semiconducting to metallic at a critical temperature (T_c). During the MIT, the optical properties are also changed, and such vanadium oxides are called chromogenic materials. This change of colour under an external stimulus either by photon radiation, temperature and voltage can be further defined as photochromic, thermochromic and electrochromic effect [45]. The value of T_c depends on the vanadium/oxygen ratio [45, 46]. For VO_2, the critical temperature for MIT is 68 °C and it is accompanied by a reversible change in optical properties from transmissive to opaque in the IR range [47]. The electrical resistivity of VO_2 is about 20 Ω·cm in the semiconducting phase to about 0.1 Ω·cm in the metallic phase

[48]. This change of optical and electrical properties is due to a change in the crystal structure of VO_2 *i.e.* from metallic IR-transparent monoclinic VO_2(M) to semiconducting IR-translucent tetragonal rutile VO_2(R) (Figure 2). Since the switching time between the two phases at T_c is considered as fast, vanadium dioxide is an excellent candidate for smart applications. It is the case of intelligent windows which can save energy consumption, thus reducing emission of greenhouse gases [11].

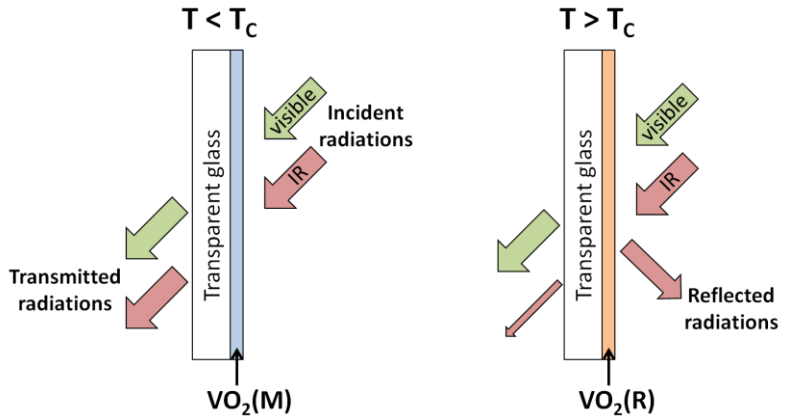

Figure 2. Principle of VO_2 thermochromic coating deposited on transparent support [36].

Vanadium pentoxide (V_2O_5) is also used in some concrete applications. It is a known catalyst in the selective oxidation of various organic compounds such as methanol into formaldehyde, butane into maleic anhydride, etc. and in the preparation of sulphuric acid by catalysing SO_2 into SO_3 [39, 49, 50]. V_2O_5 is also used as promising electrode material for lithium-ion batteries (LIBs) since it has a layered structure and high theoretical energy density (1.1 $kW{\cdot}h{\cdot}Kg^{-1}$) which corresponds to a capacity of 440 $mA{\cdot}h{\cdot}g^{-1}$ for fully lithiated V_2O_5 *i.e.* $Li_3V_2O_5$ [51, 52]. However, the charging of large amount of Li ions irreversibly change the structural properties of V_2O_5 [53]. For one lithium (LiV_2O_5), the lattice structure is extremely reversible with over 1000 cycles without capacity loss [54]. It is worth noting that Panasonic has commercialized vanadium pentoxide as cathode material in rechargeable LIBs. Such a cathode can be used only for low-energy application because of kinetic problems [55]. Therefore, other vanadium oxides like metastable V_6O_{13} have to be used since it exhibits higher capacity (420 $mA{\cdot}h{\cdot}g^{-1}$) and more Li ions can be inserted in the layered structure of

V_6O_{13}: 8 mol of Li^+ for 1 mol of V_6O_{13}. However, the drawback of this vanadium oxide as cathode material in LIBs is the poor cycling performance [56].

Vanadium oxides are also interesting for microelectronic applications. That is the case of VO_2, V_2O_3 and V_2O_5 which are stable oxides containing vanadium in a single oxidation state. Indeed, these compounds are chromogenic with reversible changes in their physical properties at T_c which is illustrated by the typical hysteresis loop of the MIT. The width of this loop is a crucial parameter for microelectronic applications. For instance, vanadium oxides are well known materials for bolometers (a bolometer is a thermal IR detector), especially for imaging as thermal camera, night vision camera, mine detection, fire detection and gas leakage detection [57]. Vanadium oxides, especially V_2O_3, are excellent candidates for bolometers since high temperature coefficient of resistance (TCR) and a small noise constant (1/f) are required [57]. V_2O_3 has the advantage to have MIT with a critical temperature which is far below the room temperature, thus resulting in a very low level of noise. It is worth noting the use of vanadium oxides in bolometric applications appeared after 1992, since prior to this date, it was classified by the US government for military purposes.

As an overview, the advantages of vanadium oxides are attractive materials due to their easy way of fabrication which is inexpensive, non-toxic and imply scalable wet chemical techniques [58]. For example, V_2O_5 is a yellow-brown compounds which can be prepared by calcination of vanadium metal powder in an excess of oxygen or by thermal decomposition of ammonium metavanadate (eq. 1). On the other hand, V_6O_{13} can be obtained by partial reduction of vanadium pentoxide using ammonia (eq. 2).

$$2NH_4VO_3 \rightarrow V_2O_5 + 2NH_3 + H_2O \qquad (1)$$

$$9V_2O_5 + 4NH_3 \rightarrow 3V_6O_{13} + 2N_2 + 6H_2O \qquad (2)$$

Beside the above-mentioned applications of vanadium in various technologies, vanadium oxides can be also used in photochemical processes for environmental purposes (see next section). That highlights again the versatile and multivalent character of vanadium.

3 Photochemical processes

3.1 Pollutant removal

As mentioned in the environmental context, the contamination of the hydrosphere by the release of inefficiently treated wastewaters is a critical issue. Many organic pollutants are accumulated in water, especially the persistent organic pollutants (POPs) and the contaminants of emerging concern (CECs), *i.e.* pharmaceuticals and personal care products (PPCPs), endocrine-disrupting compounds (EDCs), etc., thus requiring the development of efficient treatments for wastewater treatment plant (WWTP) effluents. Indeed, the discharge of treated WWTP effluents is the main source of contamination of CECs and POPs into the natural environment, thus being a real threat for drinking water (*i.e.* ground and surface waters) and impacting not only the ecosystem, but also the human health [59].

One of the most promising techniques to treat water from organic contamination is the advanced oxidation process (AOP). The AOPs are based on the generation of reactive oxygen species (ROS) including inorganic radicals such as the hydroxyl radical ($HO^{\bullet}$). AOPs can degrade completely organic molecules into full mineralization (*i.e.* into H_2O, CO_2, etc.) but also they can enhance the biodegradation of some organic pollutants [59]. The activation of the AOPs can be performed either by catalysis, thermolysis, photolysis or a combination of these means.

Photo-induced AOPs are a class of processes which are interesting since it involves the use of light. Among them, photolysis, photocatalysis and photo-Fenton are the most investigated. Photolysis is based on the sole use of light to (i) break the chemical bonds in the organic molecule or (ii) to activate the generation of inorganic radicals by activation of precursors (H_2O_2 and $S_2O_8^{2-}$). However, UVB and UVC irradiations are the most used lights, thus photolysis cannot be considered as a good alternative. On the other hand, photocatalysis and photo-Fenton are techniques that combine catalytic compound with light radiation and are considered as the most viable technique since it can involve "green" materials and the use of natural solar light, thus being sustainable and environmentally friendly.

In AOPs, the main reactive species are hydroxyl radicals ($HO^{\bullet}$). This inorganic radical is a strong oxidant with a redox potential $E^{0}(HO^{\bullet}/H_2O)$ of 2.8 V *vs.* SHE, and it reacts

nonselectively with most of the organic contaminants at high bimolecular kinetic constants (10^8–10^{11} $M^{-1}\cdot s^{-1}$). These characteristics of $HO^\bullet$ are responsible for the high efficiency of AOPs in the removal of POPs and CECs [60]. The reaction between hydroxyl radicals and organic molecules proceeds mainly by hydrogen abstraction and by hydroxyl addition to unsaturated bonds. It is worth noting that the involvement of hydroxyl radicals in organic decontamination process is not easy to demonstrate since the half-life of $HO^\bullet$ is in the order of nanosecond. Therefore, most of their identification are performed using indirect methods such as fluorescence spectroscopy or electron paramagnetic resonance in the presence of suitable probe molecules. Besides hydroxyl radicals, the photo-induced degradation of organic pollutants involves other primary inorganic radicals like the superoxide anion radical ($O_2^{\bullet -}$) and its conjugated form, the hydroperoxyl radical ($HO_2^\bullet$). These radicals are, however, less reactive than $HO^\bullet$ [60].

3.1.1 Photocatalysis

The heterogeneous photocatalysis is a photo-induced process combining the use light and a semiconductor photocatalyst as, for instance, vanadium oxide-based materials. Before introducing the principles of heterogeneous photocatalysis, let's introduce basics about semiconductors which can be used as photocatalysts. The term "semiconducting" was first used by Alessandro Volta in 1782 while Johan Koenigsberger started to classify materials into conductor, insulator and semiconductor at the beginning of the XX^{th} century. But it is in 1874 that the concept of photo-conductivity appeared where, under incident light of sufficient energy, the electrons can move from valence band (VB) to conduction band (CB) while holes have an opposite motion, thus generating a current [61]. Indeed, when the supplied energy to the semiconductor is higher than the energy bandgap (E_g - also known as forbidden energy band, which is the energy gap separating the VB to the CB), an electron can move from VB to CB [61]. The value of the energy bandgap is an intrinsic value of the semiconductor, thus varying according to the chemical composition of the materials but also its crystal structure. Therefore, a key parameter in the selection of a semiconductor photocatalyst is the value and the energy position of E_g.

The basic principle of heterogeneous photocatalysis (*i.e.* using semiconductors) is based on the generation of electrons (e^-) and holes (h^+) pairs (eq. 3). Once the e^-/h^+ pairs are generated under an incident irradiation of sufficient energy ($h\nu$), *i.e.* larger than E_g, they can react with water and oxygen to form primary reactive oxygen species (ROS) as described in eqs. 4-6, that subsequently degrade the organic pollutants. The mechanism of ROS is based on the adsorption of water molecule (in the form of surface hydroxyl) and oxygen, that then react with photogenerated holes and electrons reaching the surface of the photocatalyst. The formation of ROS also the transformation of primary ROS ($HO^\bullet$ and $O_2^{\bullet-}$), thus leading to hydroperoxyl radicals ($HO_2^\bullet$) and hydrogen peroxide (H_2O_2) (eqs. 7-12). H_2O_2 is an important precursor of hydroxyl radicals but also a key species in Fenton-based processes (see next section) [9].

$$Semiconductor + h\nu \rightarrow e^- + h^+ \quad (3)$$

$$OH^- + h^+ \rightarrow HO^\bullet \quad (4)$$

$$H_2O + h^+ \rightarrow HO^\bullet + H^+ \quad (5)$$

$$O_2 + e^- \rightarrow O_2^{\bullet-} \quad (6)$$

$$O_2^{\bullet-} + H^+ \rightarrow HO_2^\bullet \quad (7)$$

$$H_2O + O_2^{\bullet-} \rightarrow HO_2^\bullet + OH^- \quad (8)$$

$$HO_2^\bullet + HO_2^\bullet \rightarrow H_2O_2 + O_2 \quad (9)$$

$$O_2^{\bullet-} + H_2O_2 \rightarrow OH^\bullet + OH^- + O_2 \quad (10)$$

$$H_2O_2 + e^- \rightarrow HO^\bullet + OH^- \quad (11)$$

$$H_2O_2 + h\nu \rightarrow 2OH^\bullet \quad (12)$$

Therefore, the degradation of organic pollutants occurs either indirectly through ROS or directly using the photogenerated charge carriers, but the indirect way is kinetically favoured due to the strong reactivity of ROS with organic molecules. However, to observe the above-mentioned photocatalytic reactions, several conditions are required. Beside the fact that the

e^-/h^+ pair generation is in competition with the recombination process (releasing the absorbed energy in the form of heat), these generated charge carriers should reach the surface of the photocatalyst where they react with adsorbed reactants (like H_2O, O_2 and organic pollutant), since photocatalysis is a surface dependent process (Langmuir-Hinshelwood model). In addition, the redox potential of the photocatalytic reaction (*e.g.* for the generation of ROS) has to lie within the energy bandgap (Figure 3). Therefore, the feasibility of a photocatalytic reaction depends mainly on the energetic position of E_g *i.e.* the positions of valence band maximum (VBM) and the conduction band minimum (CBM) of the semiconductor photocatalyst [9].

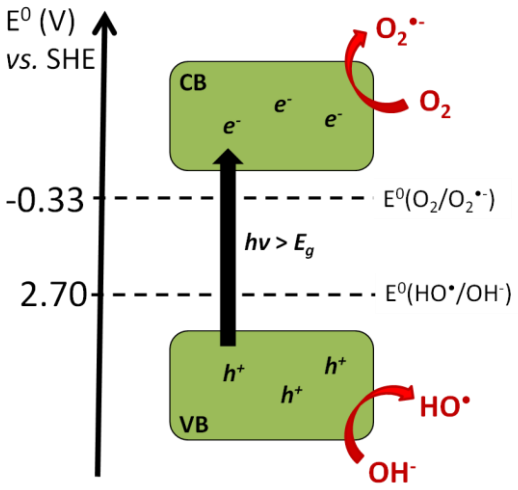

Figure 3. Mechansim of primary ROS generation by heterogeneous semiconductor photocatalysis [36].

3.1.2 Fenton-based processes

Another important photo-induced AOP is the photo-Fenton. Let's introduce all the Fenton-based reactions in order to better understand the principle of photo-Fenton. Usually, Fenton-based processes generate ROS in the presence of iron. The classical homogeneous Fenton reaction was discovered in 1894 by H. J. H. Fenton who observed the oxidation of tartaric acid in the presence of iron(II) ions and hydrogen peroxide [62]. About 100 years later, the heterogeneous classical Fenton and Fenton-like reactions were observed (eqs. 13 and 14). Compared to the homogeneous system, heterogeneous Fenton-based reactions can be used over a wider range of pH (*e.g.* environmental pH). Indeed, it is well known that dissolved Fe(II)

and Fe(III) are not stable and tend to oxidize and aggregate, thus requiring acidic pH to avoid the formation of sludge. In the form of oxides and oxyhydroxides, iron is much more stable.

$$Fe^{2+} + H_2O_2 \rightarrow [FeOH]^{2+} + HO^{\bullet} \quad (13)$$

$$Fe^{3+} + H_2O_2 \rightarrow Fe^{2+} + H^{+} + HOO^{\bullet} \quad (14)$$

However, the mechanism of heterogeneous Fenton-based reactions is still unresolved due to intricated interactions between the surface of the iron oxide/oxyhydroxide and the reactants *i.e.* H_2O_2, generated ROS and the organic pollutants (and their degradation byproducts) [60]. It is admitted the primary ROS are either generated at the surface of the materials or at the close surroundings of the surface through possibly leached iron like in homogeneous Fenton-based reactions [60]. It is worth noting the mechanism of homogeneous systems is also the matter of intense discussion in the scientific community, especially since the hypothesis of the involvement of Fe(IV) species.

In Fenton-based processes, it is accepted that the limiting step is the regeneration of Fe(II) from Fe(III), thus implying a catalytic cycle between these 2 species. To support this iron cycle, the photo-Fenton reaction is considered as viable alternative to classical Fenton and Fenton-like reactions. In homogeneous system, the generation of ROS such as hydroxyl radicals occurs *via* the photolysis of iron (III) species, especially in the $[Fe(H_2O)_5(OH)]^{2+}$ complex, through ligand to metal charge transfer (LMCT). In heterogeneous system, photolysis of surface hydroxyl group is admitted (eq. 15). The photo-induced AOP triggered by heterogeneous photo-Fenton reaction is promising for the efficient degradation of organic pollutants since it allows the use of solar light and no addition of H_2O_2 is required, thus increasing the sustainability of such a process [63, 64].

$$[Fe\ (OH)]^{2+} + h\nu \rightarrow Fe^{2+} + HO^{\bullet} \quad (15)$$

Other transition metals can also trigger Fenton-based processes, especially by using elements that are abundant in the earth crust. Intense research is focused on these iron-free Fenton-based processes [65]. For example, aluminium can convert H_2O_2 into $HO^\bullet$ through e^- transfer (Figure 4). However, the main disadvantage of using zero-valent aluminium is the formation of Al_2O_3 layer which requires strong acidic conditions to remove it and to avoid the inhibition of the Fenton process. In absence of H_2O_2, the mechanism of ROS generation implies the *in-situ* production of hydrogen peroxide by electron transfer to dissolved oxygen. The hydrogen peroxide is then subsequently decomposed to generate hydroxyl radicals (Figure 4) [65].

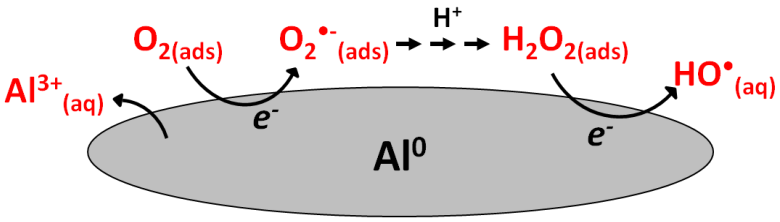

Figure 4. Generation of primary ROS at the surface of aluminium [36].

Another element with high natural occurrence and which can trigger Fenton process is manganese. Mn is interesting due to its versatility in oxidation states ranging from 0 to +VII. Among them, only Mn(II), Mn(III) and Mn(IV) are relevant for the removal of organic contamination in water. Mn(II) species are predominantly present in soluble form while Mn(III) and Mn(IV) exist in the form of oxides and oxyhydroxides such as Mn_3O_4, Mn_2O_3, MnOOH and MnO_2. The latter is already known oxidant for the degradation of adsorbed organic pollutant without the use of light or H_2O_2. The mechanism of Mn-mediated Fenton process is intricated and it is not yet resolved. However, it is assumed that hydrogen peroxide is activated by interconversion between Mn^{2+} and Mn^{4+} *via* intermediate Mn^{3+}. According to the type and the form of the oxide/oxyhydroxide, the main ROS are hydroxyl radicals and superoxide anion radicals. The main advantage of this iron-free Fenton process is a significant efficiency at circum-neutral conditions, which is relevant for real wastewater treatment [65].

Copper is also an important element for iron-free Fenton process due to an analogous mechanism as in the case of iron. Like Fe(II) and Fe(III), Cu(I) and Cu(II) can generate ROS, especially $HO^{\bullet}$ and $HO_2^{\bullet}$, by activation of H_2O_2 (eqs. 16 and 17). In the form of oxides, the main advantage of copper over iron is the limited leaching of Cu. However, a strong disadvantage of copper is the instability of Cu_2O under light and humidity. Therefore, an excess of H_2O_2 must be used in the presence of CuO, but it decreases the efficiency of the Fenton reaction by scavenging of ROS [65].

$$Cu^{2+} + H_2O_2 \rightarrow Cu^{+} + H^{+} + HOO^{\bullet} \qquad (16)$$

$$Cu^{+} + H_2O_2 \rightarrow Cu^{2+} + OH^{-} + HO^{\bullet} \qquad (17)$$

A well know Fenton active element is cerium. It is the only lanthanide which can trigger Fenton processes either in soluble (Ce^{3+} and Ce^{4+}) or solid form (CeO_2). The mechanism is similar to that of iron (eqs. 18 and 19). But considering the toxicity of cerium, it cannot be implemented in applications for the treatment of organic pollution in water [65].

$$Ce^{3+} + H_2O_2 \rightarrow Ce^{4+} + OH^{-} + HO^{\bullet} \qquad (18)$$

$$Ce^{4+} + H_2O_2 \rightarrow Ce^{3+} + H^{+} + HOO^{\bullet} \qquad (19)$$

Finally, vanadium is also an element which is active in Fenton processes. Like Mn, vanadium exhibits versatile stable oxidation states, but only V(V) and V(IV) in the form of oxo-cations can generate ROS from H_2O_2 as observed in eq. 20 [66]. Heterogeneous Fenton processes might be also activated using vanadium oxides.

$$VO^{2+} + H_2O_2 \rightarrow VO_2^{+} + H^{+} + HO^{\bullet} \qquad (20)$$

Although classical Fenton and Fenton-like processes have been studied for all these metals, the photo-Fenton process has not been yet clearly demonstrated. It is a hot topic which is intensively investigated within the scientific community, and soon significant results will probably confirm the feasibility of such a photo-induced process.

3.2 Energy production

Beside the remediation of organic pollution in water, the production of renewable and sustainable energy also belongs among the main environmental challenges of the Mankind [67, 68]. To this end, the conversion of solar energy is promising since it is considered as clean and infinite. The solar light can be utilized in the production of green energy *e.g.* electricity through photovoltaic technology and hydrogen through photochemically assisted water splitting [61]. Let's focus on the production of hydrogen since it is the future fuel for the next generations. Hydrogen (H_2) has a great energy yield compared to fossil fuels (120 $KJ{\cdot}g^{-1}$ *vs.* 40 $KJ{\cdot}g^{-1}$). In addition, the consumption of hydrogen fuel releases only water while fossil fuels produce greenhouse gases and particulate matter. So far, H_2 can be produced by steam methane reforming or water electrolysis but these techniques are not economically viable and environmentally friendly. A promising way is the photochemically assisted water splitting using semiconductor photocatalysts. The water splitting using solar light, *i.e.* conversion of solar energy into chemical energy, has been stated as the "Holy Grail" in the field of energy by the scientific community [11]. However, the Gibbs energy for overall water splitting (eqs. 21-23) is high (ΔG^0 = 237.2 $KJ{\cdot}mol^{-1}$), and the energy provided by the solar light combined with currently commercially available photocatalysts is not enough to produce hydrogen and oxygen from water. Unless the discovery of an extraordinary efficient, green and inexpensive photocatalyst, additional energy should be supplied [69, 70, 71, 72]. An alternative and viable solution is the combination of electrical energy with photocatalyst deposited in the form of an electrode. This strategy appears, so far, the best one to produce hydrogen from water splitting since it saves energy compared to other methods including water electrolysis. Such a system is called a photoelectrochemical (PEC) process *a.k.a.* electrochemically assisted photocatalysis (electrophotocatalysis) (Figure 5). Using PEC system, entirely green hydrogen can be produced by using electricity from photovoltaic technology.

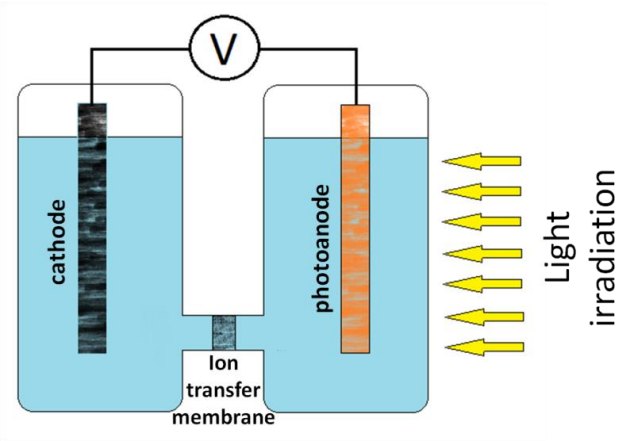

Figure 5. Two-compartment photoelectrochemical cell: the case of photoactive anode [36].

$$4H^+ + 4e^- \rightarrow 2H_2; \qquad E^o = 0\ V \qquad (21)$$

$$2H_2O + 4h^+ \rightarrow O_2 + 4H^+; \qquad E^o = +1.23\ V \qquad (22)$$

$$2H_2O + h\nu \rightarrow 2H_2 + O_2\ ; \qquad \Delta E = 1.23\ V \qquad (23)$$

The first report on PEC water splitting dates 1972 where Fujishima and Honda used a two-compartment cell with rutile TiO_2 as photoanode and UV as light source [73]. Therefore, a PEC system is basically a cell composed of an anode and a cathode and coupled to a potentiostat that can apply an electrical voltage between the electrodes. There are several PEC cell configurations with either electrodes in the same compartment or separated by an ion-transfer membrane.

For water splitting, the two-compartment PEC cell is the most suitable configuration since O_2 and H_2 can evolve separately, thus avoiding potential explosive mixture and back recombination into water (Figure 5) [74]. In such a PEC cell equipped with a semiconductor photocatalyst as an electrode, the requirements for feasible water splitting are that the redox potentials for both water oxidation (eq. 22) and reduction (eq. 21) should lie within the energy bandgap of the photocatalyst (Figure 6) [70, 71, 72, 74, 75]. Therefore, the PEC water splitting process can be summarized as the following: *(i)* water oxidation in the photoanode

compartment, *(ii)* e^- transfer through external circuit toward the cathode compartment where *(iii)* reduction of water occurs [70, 74].

The photocatalyst is often a n-type semiconductor, like for instance most of the vanadium-based oxides, thus it is called a photo-anode. For overall water splitting, ΔE = 1.23 V, so theoretically the energy bandgap of the should be at least 1.23 eV to generate e^- and h^+ of sufficient energy to trigger the oxidation and reduction of water (eqs. 22 and 21) [75]. However, due to overpotential losses, the value of E_g should be at least 2 eV [69, 70, 71, 72].

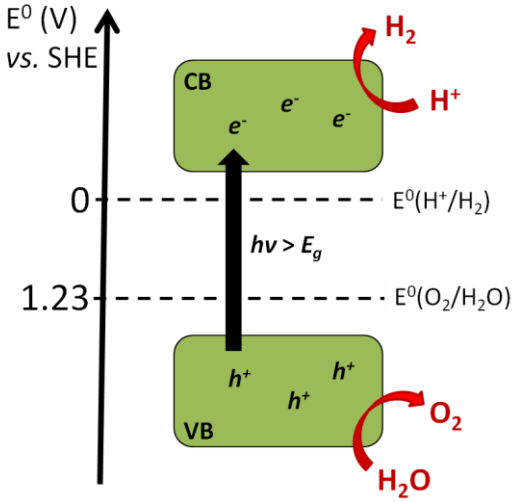

Figure 6. Mechansim of overall water splitting using heterogeneous semiconductor photocatalysis [36].

4 Structure and properties of vanadium-based oxides

4.1 Binary oxides

4.1.1 Generalities

In the form of binary oxides, vanadium is stable at different oxidation states and exhibits single valence state in VO, V_2O_3, VO_2 and V_2O_5, and mixed valence states like in V_4O_7, V_4O_9 and V_6O_{13}. The preparation of these vanadium oxides depends strongly on the synthesis parameters including the temperature and the partial pressure and composition of annealing atmosphere [52]. For instance, V_2O_5 can be prepared from VO_2 after annealing in oxidative atmosphere. During the formation of V_2O_5, other phases are formed and transformed

according to the following order: VO_2, V_6O_{13}, V_4O_9, V_3O_7 and V_2O_5. The intermediate oxides are mixed valence oxides with an average oxidation state of 4.3 for V_6O_{13}, 4.5 for V_4O_9 and 4.7 for V_3O_7, and they belong to Wadsley series *i.e.* oxides of general formula V_nO_{2n+1} [51, 76, 77]. Another important category of vanadium oxides is the Magnéli phases which have a general formula of V_nO_{2n-1} [51].

Binary vanadium oxides exhibit a wide variety of crystal structures due to many stable oxidation states this transition metal, thus leading to a rich coordination of vanadium [78]. The electronic properties of vanadium oxides are related to their crystal structure [51, 79]. Usually, in transition metal oxides, the s-orbital of the transition metal and the p-orbitals of the oxygen are pushed away from the Fermi level while the d-orbitals remain close to this level [80]. Consequently, the d-orbitals of vanadium govern the electronic properties in vanadium oxides. These properties are described using either the crystal field theory or the conventional band theory. Using the crystal field theory, the splitting energy of the molecular orbitals is about 1-2 eV and such values increases with the oxidation state of the metal. In the band theory, the d-orbitals contribute mainly to the conduction band while the oxygen 2p-orbital form the valence band (for transition metal of the 3d series like vanadium). Since such metal oxides are semiconductors, it is considered that the VB is filled in electrons while the CB, which separated by the energy bandgap, remains empty.

The electronic properties are of significant importance to understand the performance of the different binary oxides in applications such as the photochemical processes. To discuss in detail the properties of vanadium oxides, the band theory is used along this chapter. This theory leads to the schematic representation of transition metal oxides as semiconductor in the form of an electronic band structure diagram which is the plot of the electron energies against the wave vector. The number of electronic bands the diagram is equal to the number of atomic orbitals in the unit cell of the metal oxide. In the diagram, the bandwidth (or the band dispersion) is the energy difference between the lowest and highest levels in a band and it corresponds to the overlap between the interacting orbitals. So, greater the overlap, greater the bandwidth. As a result, different diagrams are obtained for insulator, semiconductor and metallic materials such as in Figure 7 where only the electronic band that are the closest to the Fermi level are represented. Based on such diagrams, the electronic properties of metal oxides are microscopically investigated, thus helping the discussion of

other properties of material [81]. For instance, for metal oxide semiconductors, optical properties can be estimated since the required energy value of the incident light stimulus to allow electron transition from VB to CB can be determined. In other words, the energy bandgap (E_g) can be calculated and it is a parameter of high interest for many applications, especially for photocatalysis. Concerning binary vanadium oxides, their electronic band structures are characterized by a strong hybridization of oxygen 2p-orbitals and vanadium 3d-orbitals. The valence band is predominantly formed by oxygen orbitals while the conduction band is composed mainly of vanadium orbitals.

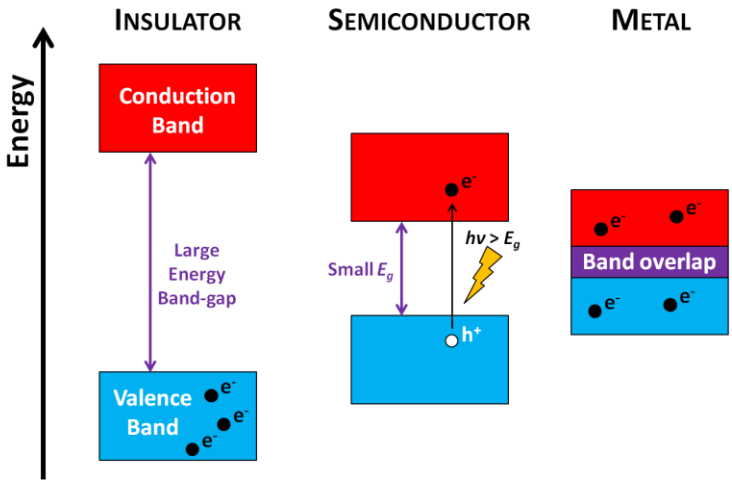

Figure 7. The band structures of insulator, semiconductor and metal [36].

Most of the binary vanadium oxides exhibit a metal-to-insulator transition along with chromogenic properties, thus being promising advanced materials. The V-O bonds have an ionic character, thus the critical temperature of the MIT depends strongly on the oxidation state of vanadium [45]. The MIT in binary vanadium oxides is accompanied by changes in optical, electrical and magnetic properties, that are the results of the reversible crystal structure transition. Indeed, the displacement of the atoms in the crystal lattice leads to a change in the electronic band structure of the material [82]. The degree of anisotropy in vanadium oxides, *i.e.* the difference in physico-chemical properties based on the direction, increase according to the following order: $V_2O_3 < VO_2 < V_2O_5$, where vanadium pentoxide has a layered structure. It is worth noting that vanadium monoxide (VO) also exists but as a non-stoichiometric oxide. Vanadium monoxide crystallizes in cubic rock salt structure (NaCl) [83].

4.1.2 V_2O_5

Vanadium pentoxide contains V with an oxidation state of +V and this oxide is at one end of the Wadsley series. V_2O_5 has a melting point of 690 °C and it exhibits an orthorhombic crystal structure which belongs to the space group P_{mmn} [84]. The crystal structure of vanadium pentoxide is composed of *[VO_5]* square pyramids which form alternating double chains along the *c*-axis. These double chains are connected laterally by bridging oxygens to form a sheet in the *a–c* plane. The planes themselves are connected by Van der Waals bonds along the *b*-axis (Figure 8) [58]. Therefore, V_2O_5 has a layered structure which is relatively permeable, thus allowing intercalation of small cations. In addition, the surface of V_2O_5 sheets is polar and hydration phenomenon can occur easily [85]. In addition, the theoretical nominal valence state of vanadium atoms in V_2O_5 is +V, but in practice, the thermal agitation and the crystal defects create a small concentration of vanadium(IV). Consequently, small lattice distortions are present in the V_2O_5 crystal structure which favours the electronic conductivity within V_2O_5 sheets by the phenomenon of electron hopping [58].

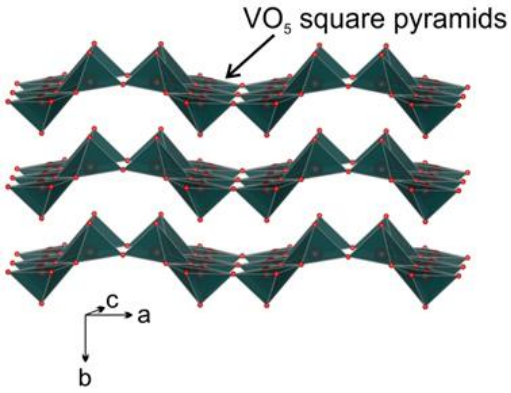

Figure 8. Layered structure of V_2O_5 [86].

Concerning the electronic band structure of V_2O_5, theoretical calculations using the density functional theory (DFT) have shown that the Fermi level is at about 1.6 eV while the conduction band minimum and valence band maximum are at about 1.0 eV and 2.7 eV, respectively, thus the energy bandgap is 1.7 eV which is an indirect E_g [87]. However, DFT

calculations underestimate the value of the energy bandgap since experimentally, E_g is measured at 2.3 eV. The electronic band structure of V_2O_5 also exhibits 2 discrete intermediate bands within the energy bandgap with narrow bandwidth (about 0.7 eV) [87]. These intermediate bands are responsible of better charge transport properties in V_2O_5 structure, but also contribute to multi-optical transitions from VB to CB.

Vanadium pentoxide exhibits interesting optical and electrical properties which are anisotropic. This anisotropy in V_2O_5 is due to strong hybridization, thus leading to highly dispersive electronic bands and ultimately to structural anisotropy. Regarding the electronic conduction, it is significantly higher within the *a-c* plane than the conduction perpendicular to these planes [87]. Indeed, the phenomenon of electron hopping is much easier with the sheets due to shorter distances between vanadium atoms while electron motion is more difficult between the sheets that are stacked by Van der Walls bonds. Therefore, the in-plane conductivity is evaluated from 10^{-2} to 10^{-3} $S \cdot cm^{-1}$ which is a relatively high value for a semiconductor [88]. Regarding the optical transmittance, V_2O_5 is transparent in near-UV and the blue part of visible spectrum, and opaque in near-IR and the red part of visible spectrum. However, vanadium pentoxide is a well-known electrochromic material, thus changing its optical properties under an electrical stimulus. The electrochromic transitions under a voltage show an excellent reversibility, and V_2O_5 films are coloured at -1 V while the colour is bleached at +1 V [89]. V_2O_5 is unique in the sense that it is difficult to classify this oxide in the category of either anodic or cathodic electrochromism. Cathodic electrochromism refers to a decrease in transmittance caused by charge injection (like titanium and tungsten oxides), and anodic electrochromism is the opposite *i.e.* a decrease in transmittance (like manganese and iron oxides). Vanadium pentoxide has simultaneously a increased transmittance in near-UV and blue visible region and a decreased transmittance in near-IR and red visible region by charge injection [90]. The charge injection can be also performed by intercalation of small cations such as Li^+ and Na^+ between the a-c sheets of the V_2O_5 structure. Such an intercalation causes electrochemical charge transfer reactions. Due to its excellent electrochromic properties, V_2O_5 has been already developed for the design of smart windows. It is worth noting that vanadium pentoxide is also a thermochromic material with a transition at about 260 °C, but only in the form of thin films since bulk V_2O_5 remains semiconducting no matter the temperature [91, 92].

4.1.3 VO_2

Vanadium dioxide contains V with an oxidation state of +IV and this oxide is at one end of the Wadsley series. VO_2 has a melting point of 1967 °C and presents a wide variety of polymorphs: more than 10 types of VO_2 phase have been already reported. Therefore, the preparation of the desired polymorph is a hard task because most of their structures are similar as well as the experimental conditions required for their synthesis. The main investigated vanadium dioxide phases are VO_2(M), VO_2(R) and VO_2(B) while other polymorphs like VO_2(A), VO_2(C) and VO_2(D) are less interesting for potential applications [93, 94]. The VO_2(A), VO_2(B), VO_2(C) and VO_2(D) are metasable phases and usually required lower annealing temperature for their preparation than the stable VO_2(M) and VO_2(R). Vanadium dioxide exhibits MIT with T_C at 68 °C where VO_2(M) and VO_2(R) are semiconducting and metallic phases, respectively. Below the critical temperature, VO_2(M) has a monoclinic structure while above T_C, VO_2(M) is reversibly transformed into rutile VO_2(R) [45, 95].

The crystal structures of VO_2(M/R) are represented in Figure 9. The monoclinic VO_2 belongs to the space group $P2_1/c$ while the rutile VO_2 has a tetragonal unit cell of space group $P4_2/mnm$. Both the crystal structures are composed of $[VO_6]$ octahedra as building units since each vanadium has a coordination number of 6 [58]. The metastable VO_2(B) can be also labelled VO_2(M2) since it has also a monoclinic structure, and it can be converted to either VO_2(A) or VO_2(M) according to the annealing parameters of the heat treatment [84]. The main structural differences between VO_2(M) and VO_2(B) is based on angles in the unit cell where β is 122.62° in VO_2(M) and 92.88° in VO_2(B). Also, compared to VO_2(M), VO_2(B) does not exhibit an MIT.

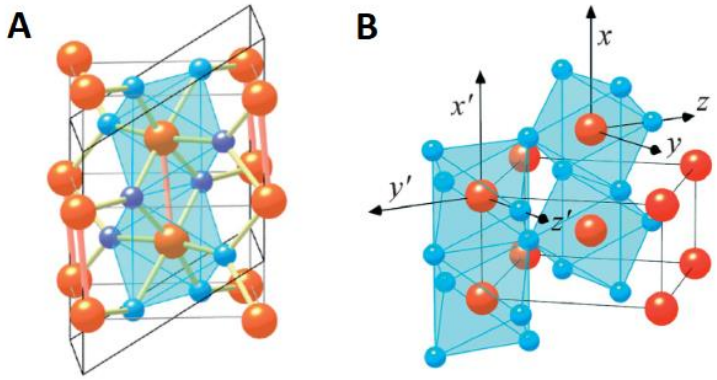

Figure 9. Crystal structures of (A) semiconducting VO_2(M) and (B) metallic VO_2(R) [96]. The bigger red spheres are vanadium atoms and the smaller blue ones are oxygen.

The metal-to-insulator transition between VO_2(M) and VO_2(R) phases can be induced by a temperature gradient, thus leading to a significant change in electrical properties. The MIT is accompanied with structural changes where vanadium pairs are dimerized in VO_2(M) [51]. This dimerization is responsible of the semiconducting character of the monoclinic phase while in the rutile, the vanadium 3d-orbitals are shared by all the V atoms that gives rise to metallic behaviour [97]. It is worth noting both the phases have similar crystal lattices, but the main difference is the slight changes in the position of vanadium atoms. The structural changes between VO_2(M) and VO_2(R) are schematized in Figure 10. Beside dimerization of vanadium in VO_2(M), twist from linear to zigzag-type chains vanadium chain occurs. Therefore, the local structural rearrangement of vanadium atoms confirms its key role in the modification of the electronic structure, especially the value of the energy bandgap [51].

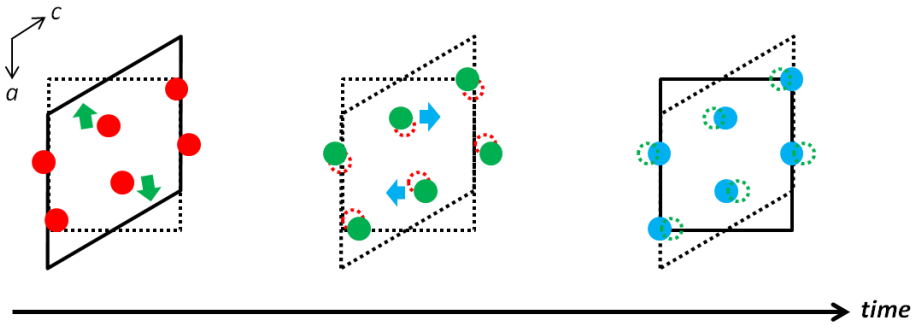

Figure 10. Changes in the crystalline structure during VO_2 phase transition. The schematized sequence occurs in the picoseconds scale [36].

Concerning the electronic band structure of VO_2(M/R), the Fermi level in both the phases is almost at the same energy level *i.e.* at 7.47 eV for VO_2(R) and 7.44 eV for VO_2(M) [45]. In addition, VO_2(M) and VO_2(R) present the same number of band groups, but in the rutile phase each group is doubled, thus leading to an overlap between the valence and the conduction bands *i.e.* to metallic behaviour [45]. By using the crystal field theory, the vanadium 3d-orbitals in VO_2(M/R) are split into doubly degenerated e_g and triply degenerated t_{2g} levels [45]. Since the e_g orbitals are directed towards the oxygen 2p-orbitals, they are labelled as e_g^{σ} bands while for the t_{2g} orbitals, which are not directed toward the oxygen orbitals, form e_g^{π} and a_{1g} bands (Figure 11). In the VO_2(M), dimerization of vanadium from lattice distortion leads to the splitting of a_{1g} into 2 bands. In addition, the e_g^{π} band is more destabilized in VO_2(M) due to stronger V-O overlapping and it pushes this band upwards from the Fermi level [98, 99]. Consequently, there is no overlap between a_{1g} and e_g^{π} bands at the Fermi level. In VO_2(R), there is no dimerization, thus no splitting of a_{1g} band occurs, and therefore, the overlapping between the a_{1g} and e_g^{π} bands at the Fermi level is responsible of the metallic properties of VO_2(R) (Figure 11). Experimentally, the energy bandgap is measured about 2.5 eV in the semiconducting monoclinic VO_2 while it is 0.6 eV in the metallic rutile phase [100].

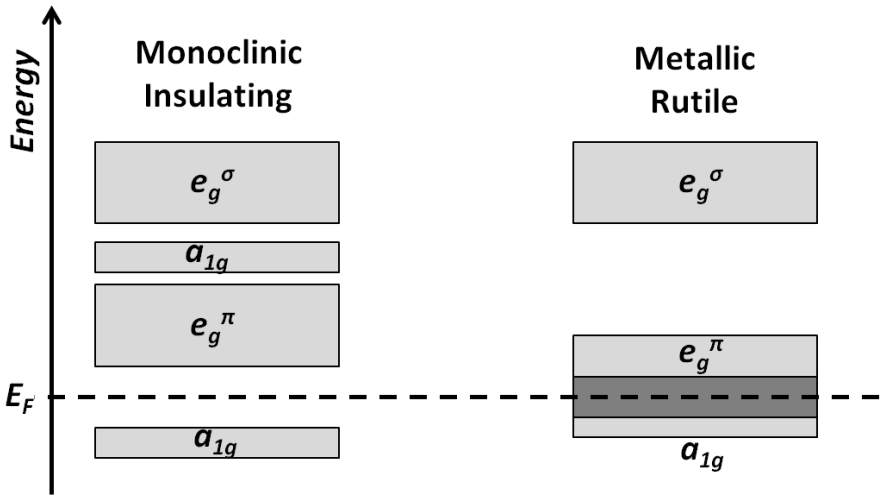

Figure 11. Energy diagrams of semiconducting(insulating) monoclinic and metallic rutile phases of VO_2 [36].

Concerning the optical properties of vanadium dioxide, there is a significant anisotropy in the IR region [45]. Indeed, at $T > T_c$, VO_2(R) is transparent in the IR region and the optical

transmittance changes by about two orders of magnitude during the MIT [101]. The MIT exhibits a hysteresis loop where the optical switching in the IR region occurs at 80 °C upon heating and 60 °C upon cooling. In the visible range, VO_2(M/R) phases absorb light and both the bulk phases are brown-yellow. In the form of thin films, the colour turns into red-brown for VO_2(M) and green-blue for VO_2(R) [102]. Like V_2O_5, VO_2(M/R) is electrochromic thus changing it optical properties in the response of a voltage, but VO_2(M/R) has better thermochromic properties [103].

The MIT in VO_2(M/R) can be controlled using different means than using voltage or temperature. For instance, laser pulse is an effective method that can provide sufficient energy to trigger an ultra-fast and non-thermal MIT [104]. Another example to regulate the MIT is by using the strains in VO_2(M/R). Indeed, deposited in the form of film, the lattice and elastic mismatches between VO_2 and the substrate is a source of strain which can adjust the MIT by causing a change of the transition temperature [105]. Also, the MIT can be controlled by using chemical doping in the structure of vanadium oxide, thus either decreasing or increasing the value of T_C according to the type of dopant [117]. Indeed, insertion of discrete energy levels within the energy bandgap can arise using n- or p-type dopants, thus leading to electrons and holes injection and holes injection in CB and VB of VO_2, respectively. Doping by W(VI) decreases the T_c of MIT while low-valence metal ions such as Cr^{3+}, Ga^{3+} and Al^{3+} are used to increase the critical temperature [106, 107, 108].

4.1.4 V_2O_3

Vanadium sesquioxide contains V with an oxidation state of +III and V_2O_3 has a melting point of 1970 °C. Due to the low valence of vanadium, there are a limited number of V_2O_3 phases. Intense research is ongoing to discover new polymorphs of V_2O_3 that are similar to those of iron(III) oxide like α-Fe_2O_3, β-Fe_2O_3, γ-Fe_2O_3, δ-Fe_2O_3 or ε-Fe_2O_3 [109]. So far, only δ-V_2O_3 and ε-V_2O_3 have not been yet discovered.

Like vanadium pentoxide and dioxide, V_2O_3 also exhibits MIT with a change of crystal structure at T_C between low-temperature monoclinic and high-temperature corundum [45]. Below at T_C *i.e.* in semiconducting state, vanadium sesquioxide has body centred monoclinic structure with space group *I2/a* while in the metallic state, V_2O_3 has trigonal corundum

structure with space group $R\bar{3}c$. the critical temperature is relatively low where a striking MIT accompanied by a jump in resistivity (by seven orders of magnitude) is observed at about 150 K. Therefore, at room temperature, corundum V_2O_3 exhibits a metallic behaviour due to a finite overlapping of the valence and conduction bands (the value of E_g was experimentally measured at 0.66 eV).

Concerning the electronic band structure, the Fermi level of V_2O_3 is estimated at 9.2 eV. Using the crystal field theory, the vanadium 3d-orbitals can be considered in an octahedral symmetry since the crystal structures are based on *[VO_6]* units, thus leading to a splitting into t_{2g} and e_g^{σ} (like in the case of VO_2). Due to monoclinic and corundum structure, the t_{2g} band is split into a_{1g} singlet and doubly degenerated e_g^{π} bands (Figure 12). Since the symmetry is lower in the monoclinic structure, the a_{1g} and e_g^{π} bands are split, thus creating an energy gap between a_{1g} and e_g^{π} bands. In the corundum structure, there is no splitting and overlap between the a_{1g} and e_g^{π} bands occurs at the Fermi level, thus giving rise to its metallic behaviour (Figure 12) [110].

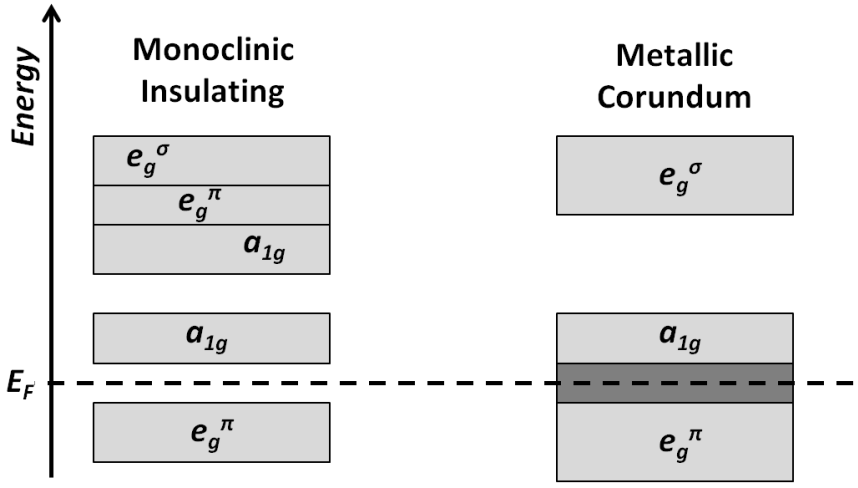

Figure 12. Energy diagrams of semiconducting(insulating) monoclinic and metallic corundum phases of V_2O_3 [36].

4.1.5 Mixed valence oxides

There are numerous binary vanadium oxides with mixed valence state. Among them, the vanadium oxides of general formula $V_nO_{(2n+1)}$ *i.e.* the Wadsley phases exist between V_2O_5 and

VO_2, while those of general formula $V_nO_{(2n-1)}$ *i.e.* the Magnéli phases exist between VO_2 and V_2O_3. Therefore, these phases have a mixture of vanadium with either +IV and +V or +III and +IV. Most of these mixed valence oxides exhibit a metal-to-insulator transition. Usually, the structure of intermediate vanadium oxides of the Wadsley and Magnéli can be described using the "shear structure" concept [111]. Using this concept, the structures are made of atomic planes of *[O]* and *[VO]* (labelled as *A* and *B*), thus composing of slabs of *[VO_2]* rutile-like structure. For the Magnéli phases, the shear operation of eliminating 1 *A*-plane every *n* *B*-plane combined to a shear vector that closes the resulting gap, the formula formula *n*VO + *(n-1)*O = $V_nO_{(2n-1)}$ is obtained [111]. Until now, 6 compounds from n = 3 to n = 8 have been isolated experimentally, and all of them exhibit MIT. On the other hand, for the Wadsley phases, similar shear operation is performed but by deleting 1 *B*-plane every *n A*-plane, thus leading to the general formula $V_nO_{(2n+1)}$. For this series, only V_3O_7 and V_6O_{13} have been obtained.

V_6O_{13} is one of the most investigated mixed valence vanadium oxides. It presents MIT with T_c = -123 °C. In his metallic state, V_6O_{13} has a layered structure belonging to space group *C2/m* while its semiconducting structure belongs to the space group $P2_1/a$. Like most of the vanadium oxides of the Wadsley series, V_6O_{13} is a promising material for cathode in rechargeable LIBs due to its layered structure and its high capacity [111, 112]. In addition, it exhibits higher rate capability, better reversible capacity, smaller volume expansion and safer lithiation potential. Indeed, due to its metallic character at room temperature, it has better performance in charge and discharge capacity and it can theoretically insert 8 mol of Li^+ ion in its structure for 1 mol of V_6O_{13}. However, the main drawback of this mixed valence oxide is its preparation since it is hard to control the V(IV)/V(V) ratio [56].

V_3O_7 belongs also to the Wadsley series, thus being an intermediate oxide between VO_2 and V_2O_5 with a V(IV)/V(V) ratio of 1/2. In the literature, this oxide is often reported in the form of hydrate *i.e.* $V_3O_7{\cdot}H_2O$. At room temperature, it is in its semiconducting phase (E_g = 2.5 eV) with an orthorhombic crystal structure of space group *Pnam* [112, 113]. $V_3O_7{\cdot}H_2O$ has a layered structure similar to V_2O_5 since it is prepared from vanadium pentoxide as precursor. It is composed of layers made of *[VO_6]* octahedra and *[VO_5]* trigonal bipyramids [111, 112, 113, 114]. Like V_6O_{13}, $V_3O_7{\cdot}H_2O$ is also a promising cathode material in LIBs due to its layered structure and high capacity [112]. In addition, $V_3O_7{\cdot}H_2O$ exhibits excellent electrochromic

performance because of optical modulation in both anodic and cathodic reactions [114]. In the form of film, $V_3O_7{\cdot}H_2O$ can switch reversibly between a reduced blue state at –1.2 V and an oxidized orange state at +1.9 V [130]. Therefore, $V_3O_7{\cdot}H_2O$ is characterized by a multi-electrochromism like V_2O_5 but with faster kinetics. Such fast kinetics can be explained by the mixed valence states in $V_3O_7{\cdot}H_2O$ that contributes to higher electronic conductivity and more active redox sites during the reduction and oxidation processes [115]. It is worth noting that non-hydrated V_3O_7 has received less attention than its hydrated form. The non-hydrated phase can be formed by heat treatment of $V_3O_7{\cdot}H_2O$ which leads to removal of the water molecule starting. However, the formed V_3O_7 is metastable and plays the role of seeds for the formation of V_2O_5. In other words, although $V_3O_7{\cdot}H_2O$ can be prepared from V_2O_5, its dehydration using heat treatment gives rise to its oxidation into V_2O_5. Stable V_3O_7 has been already reported with a monoclinic crystal structure belonging to the space group *Pmmn*. Such V_3O_7 can be prepare directly by spray pyrolysis on a substrate heated at 400 °C [114].

V_4O_9 is another interesting mixed valence oxide of the Wadsley series with a V(IV)/V(V) ratio of 1. Due to this particular ratio, its preparation is a challenge. Solid-state reaction is employed by using an appropriate mixture of V_2O_5 and VO_2 in a reducing atmosphere. Also, reduction of V_2O_5 can be performed using carbon or sulphur as reducing agent under high vacuum conditions (eq. 24). However, an excess of sulphur leads to the formation of metastable VO_2(B). Indeed, both V_4O_9 and VO_2(B) have also a similar layered structure to V_2O_5.

$$4V_2O_5 + S \rightarrow 2V_4O_9 + SO_2 \qquad (24)$$

V_4O_9 has an orthorhombic crystal structure that belongs to the space group *Cmcm*. To describe its structure, the shear structure concept can be used. Let's consider V_2O_5 structure as lattice of *[V_2O_3]* layers (called "*a*") which are stacked and sharing *[O_2]* layers (called "*b*"), thus forming *[ababab…]* sequence. Based on this structure, VO_2(B) has a *[abaaba…]* stacking by using the shear operation of periodically eliminating 1 *b*-layer every two *a*-layers. It is worth noting that VO_2(B) is considered as a "daughter" structure of V_2O_5. For V_4O_9, its structure can be derived from V_2O_5 after operating 2 shear operations. The first one is to

periodically eliminate 1 *b*-layer every 4 *a*-layers, thus forming the following stacking: *[abababaababababaab…]*. The second operation is to eliminate half of the oxygen from half of the *b*-layers (labelled as *b'*), thus obtaining the following stacking: *[abab'abaab'abab'aab…]* [111]. In other words, the structure of V_4O_9 is composed of *[VO_5]* pyramids, distorted *[VO_6]* octahedra and *[VO_4]* tetrahedra. In addition, V_4O_9 is a special compound of the Wadsley series since its structure and properties are still not clearly identified. Therefore, V_4O_9 is often called "the missing link" in this series of mixed valence vanadium oxides [111].

4.2 Ternary oxides

Generally, compared to binary oxides, the advantage of ternary oxides is the possibility to tune their properties based on the presence of a third element. For example, in the case of a semiconductor d-block metal oxide doped by a p-block element, the overlap between the outer d- and s-orbitals leads to a decrease of the energy bandgap (E_g) [116]. Therefore, by extension, it is assumed that p- and d-block metals could be used to design ternary oxides with particular properties, especially photochemical ones.

Indeed, vanadium oxides are promising photocatalysts, and in the form of ternary oxides, efficient photo-response under visible light can be design for environmental applications. A well-known class of ternary vanadium oxides are the vanadates. Among them, orthovanadates, which are composed of VO_4^{3-} tetrahedral units including $BiVO_4$, $FeVO_4$, $Mn_3(VO_4)_2$ and $CeVO_4$ are widely investigated. Other vanadates like $Cu_2V_2O_7$, $Cu_3V_2O_8$, $Co_3V_2O_8$, FeV_3O_8, $Ag_4V_2O_7$ have also received attention of the scientific community. Although most of these ternary vanadium oxides do not exhibit metal-to-insulator transition, they have interesting properties for potential application in photocatalysis, LIBs, solar cells, gas sensors, etc. [117, 118, 119]. Indeed, for photocatalytic applications, these vanadates are promising since they are semiconductors with an energy bandgap in the UV and visible regions. Therefore, they can be used for environmental purposes such as the degradation of organic pollutants in water and the production of hydrogen by water splitting [120].

4.2.1 Bismuth vanadates

Bismuth vanadates exist with a wide variety of structures and most of these ternary vanadium oxides are intermediate oxides in the system Bi_2O_3-V_2O_5. The most promising bismuth vanadate is $BiVO_4$ which is a n-type semiconductor that exhibits 3 polymorphs: monoclinic scheelite-like (ms), tetragonal scheelite-like (ts) and tetragonal zircon-like (tz) phases [121, 122]. The ms-$BiVO_4$ belongs to the space group *C2/c* and has energy bandgap of 2.40 eV. The ts-$BiVO_4$ belongs to the space group $I4_1/a$ and has energy bandgap of 2.34 eV. The tz-$BiVO_4$ belongs to the space group $I4_1/amd$ and has energy bandgap of 2.90 eV [122, 123, 124, 125]. All these crystal structures are composed of $[VO_4]$ tetrahedra and $[BiO_8]$ polyhedra building units where vanadium and bismuth are at oxidation states +V and +III, respectively. In both the scheelite-like phases, each $[BiO_8]$ is surrounded by 8 $[VO_4]$, whereas in the zircon-like polymorph, Bi-based units are surrounded by 6 vanadium-based units [125]. Between monoclinic scheelite-like and tetragonal scheelite-like polymorphs, a reversible phase transition occurs at 255 °C, where ms-$BiVO_4$ is the stable phase at room temperature *i.e.* the low-temperature phase [124, 125]. In addition, between tetragonal zircon-like and tetragonal scheelite-like polymorphs, an irreversible phase transition is observed at about 400–500 °C [124, 125]. Therefore, at room temperature, there are two stable polymorphs which are ms-$BiVO_4$ and tz-$BiVO_4$. Among them, ms-$BiVO_4$ exhibits the best photocatalytic properties under solar light due to longer lifetime of the photogenerated charge carriers (*i.e.* electons and holes) and higher photocurrent. That is the result of the distorted $[VO_4]$ and $[BiO_8]$ units, thus leading to better charge carrier transport [124, 125]. Also, the E_g of ms-$BiVO_4$ is smaller than that of tz-$BiVO_4$, and it allows a better utilization of the visible light. Another advantage of $BiVO_4$ is non-toxicity.

Another parameter which should be considered to assess the photocatalytic properties of $BiVO_4$ is the exposed crystal facets. Indeed, they affect the thermodynamics and the kinetics of a chemical reaction including photochemical processes, but also the surface properties of the materials like surface adsorption of reactant and surface charge carrier transfer [123, 126]. For ms-$BiVO_4$ which is the most interesting polymorph for photocatalytic applications, the *{010}* and *{110}* crystal facets have important functions since they provide reduction and oxidation sites, respectively, in which photogenerated electrons and holes are available [127, 128]. Therefore, their investigation by photoelectrochemical (PEC) and transient absorption

spectroscopy (TAS) analyses helps to understand the photocatalytic efficiency of $BiVO_4$ [129]. The PEC measurements are quite common to discuss the behaviour of the charge carriers at the surface of $BiVO_4$, especially their surface recombination and redox properties by analysing the shape of the photocurrent curves during amperometry and voltammetry, respectively. The TAS measurements are more sophisticated but highly helpful since the dynamics of charge carriers including the relaxation and recombination rates can be monitored [129, 130]. TAS is a fast spectroscopic technique based on the sample excitation using a laser pulse followed by spectral analysis using a UV-visible spectrometer. By this mean, the optical properties of $BiVO_4$ of excited and ground states can be compared against the time at nano and even pico-second level [130]. For instance, TAS can be used to study the dynamics of photogenerated holes, that is a highly important parameter to understand the formation of hydroxyl radicals which are involved in the degradation of organic pollutants in water. Although TAS measurements will be developed to characterize semiconductor photocatalysts, studies using such a technique are scarce. However, for $BiVO_4$, TAS and PEC measurements have been published in 2014 [129, 130]. Such studies have demonstrated that there are 2 distinct mechanisms of charge carrier recombination since the time decay constants, measured by TAS and PEC, are different. One recombination process is fast (*i.e.* within microseconds) and it is assigned to bulk e^-/h^+ pair recombination while the second one is slow (i.e. within milliseconds) and it is assigned to recombination of surface-accumulated holes with bulk electrons (also called back electron transfer). Beside these characterization techniques, $BiVO_4$ exhibits several drawbacks that limit its efficiency in photocatalytic processes. Indeed, bismuth vanadate has a poor electron mobility and high e^-/h^+ recombination rate [123, 124]. In addition, $BiVO_4$ has a short hole diffusion length (70–100 nm). That is mainly due to the structure of $BiVO_4$, especially the $[VO_4]$ tetrahedra that are not connected to each other, but also its electronic properties where the vanadium 3d-orbitals are strongly localized. These disadvantages compromise the optimization of film thickness and light harvesting according to the optical penetration depth principle [124].

On the other hand, there are other bismuth vanadates that exhibit different stoichiometries and crystal structures. Among them, $Bi_4V_2O_{11}$ is one of the most investigated. It is a ternary vanadium oxide which was discovered in the 1980's. This bismuth vanadate is particularly interesting due to its properties at room temperature, especially its dielectricity,

ferroelectricity and pyroelectricity. $Bi_4V_2O_{11}$ belongs to the Aurivillius-type phases [131, 132, 133, 134, 135]. The crystal structure of $Bi_4V_2O_{11}$ is the parent structure of the *BIMEVOX* series (*BI* = bismuth, *ME* = metal substitution, *VOX* = vanadates) which are known for their attractive conduction properties at moderate temperature [132]. However, $Bi_4V_2O_{11}$ has been also studied as a promising photocatalyst [134]. $Bi_4V_2O_{11}$ exhibits two reversible phase transitions at 430 °C and at 570 °C while its melting point is at 870 °C [131, 132, 134]. Therefore, there are three polymorphs of $Bi_4V_2O_{11}$ which are the low-temperature α-phase, the intermediate β-phased, and the high-temperature γ-phase which crystallize in the monoclinic, orthorhombic and tetragonal system, respectively [133]. The space groups of tetragonal γ-$Bi_4V_2O_{11}$ and orthorhombic β-$Bi_4V_2O_{11}$ are *I4/mmm* and *Amam*, respectively [132]. For α-$Bi_4V_2O_{11}$, due to a 3-fold monoclinic supercell, it is more complicated to assign a space group, but recently, the *A2* space group has been assigned to the alpha polymorph [133]. From a structural point of view, the structure of the three $Bi_4V_2O_{11}$ phases is built from $[Bi_2O_2]^{2+}$ layers separated by vanadium–oxygen perovskite-like slabs with oxygen deficiency of general formula $[A_{m-1}B_mO_{3m+1}]^{2-}$ [131]. In these slabs *A* and *B* are vanadium, and *m* corresponds to the number of the stacked $[VO_6]$ octahedra. Therefore, for $Bi_4V_2O_{11}$ (or $Bi_2VO_{5.5}$) which is the corresponding oxygen deficient structure, *m* = 1 *i.e.* $[Bi_2O_2][VO_{3.5}\square_{0.5}]$ [132]. The main structural difference between the 3 polymorphs is the local environment of vanadium atoms in the $[VO_{3.5}]$ perovskite-like slabs [131, 133]. For example, in α-$Bi_4V_2O_{11}$, vanadium atom is surrounded by 3 different oxygen environments while in γ-$Bi_4V_2O_{11}$, there is a large disorder of the oxygen atoms. Consequently, the electrical properties of the different $Bi_4V_2O_{11}$ phases significantly differ. Indeed, the gamma polymorph exhibits the highest conductivity with 0.2 $S{\cdot}cm^{-1}$ at 600 °C, and this value strongly decrease upon phase transitions (by cooling) where the beta and gamma polymorphs have a conductivity of 0.01 $S{\cdot}cm^{-1}$ at 500 °C and 10^{-5} $S{\cdot}cm^{-1}$ at 300 °C, respectively [131]. Beside the electrical properties, $Bi_4V_2O_{11}$ has interesting optical properties for photochemical processes since the energy bandgap is about 2.15 eV, thus being promising for natural sunlight utilization. In addition, since this bismuth vanadate has a layered structure, the electronic properties are anisotropic with better e^-/h^+ pair separation rate in the stacking direction than within the layers due to short E_g, thus recombination occurs easily [135]. Another interesting characteristic of $Bi_4V_2O_{11}$ is its ability to be easily reduced to and re-oxidized from $Bi_4V_2O_{10}$.

4.2.2 Iron vanadates

Iron vanadates exist in different forms including $FeVO_4$, FeV_3O_8, Fe_2VO_4, FeV_2O_4 and $Fe_2V_4O_{13}$ [119]. These ternary vanadium oxides are intermediate oxides in the system Fe_2O_3-V_2O_5. Compared to V_2O_5, these ternary vanadium oxides exhibit higher melting point and lower decomposition rate due to the presence of Fe which stabilizes the structure, thus limiting the leaching of V. Among these iron vanadates, $FeVO_4$ is one of the most investigated and it presents a ratio V:Fe = 1 [117]. $FeVO_4$ exhibits 4 different polymorphs that are labelled as $FeVO_4$-I, $FeVO_4$-II, $FeVO_4$-III, and $FeVO_4$-IV. Except for $FeVO_4$-I which is a stable phase, all the other are metastable phases. The crystal structure of $FeVO_4$-I belongs to the triclinic system and the space group $P\bar{1}$ [118]. The structure is composed of doubly bent chains of distorted *[FeO_6]* octahedra and *[FeO_5]* trigonal bipyramids which are joined together by *[VO_4]* tetrahedra [136]. For the other $FeVO_4$ polymorphs, *i.e.* $FeVO_4$-II, $FeVO_4$-III and $FeVO_4$-IV, they possess orthorhombic $CrVO_4$, orthorhombic α-PbO_2 and monoclinic wolframite $NiWO_4$ structures, respectively [137].

$FeVO_4$-I is a stable n-type semiconductor with an energy bandgap which is calculated at 2.70 eV (for direct E_g) and 2.1 eV (for indirect E_g) [138, 139, 140, 141]. However, according to the experimental condition of the preparation of this ternary vanadium oxide, the value of E_g can fluctuate. $FeVO_4$-I is a promising photocatalyst, especially for the production of hydrogen by water splitting since its conduction band minimum is more negative than $E^o(H^+/H_2)$ = 0 V, and its high theoretical solar-to-hydrogen efficiency (which is 16%) [142]. However, the main drawbacks are its weak production of photocurrent and low incident photon-to-current efficiency (IPCE) which are 0.1 mA·cm^{-2} at 1.23 V *vs.* SHE and 1% at 400 nm [141]. Therefore, a solution is to prepare nanostructured $FeVO_4$ along with their doping by transition metal, thus increasing the specific surface area and modifying the electronic band structure of $FeVO_4$ [143]. For instance, doped $FeVO_4$ by 2% of Mo leads to a 2-fold increase of produced photocurrent, thus reaching 0.2 mA·cm^{-2}, while the IPCE increases up to 7%. At higher percentage of Mo, detrimental effect of doping is observed due to an increase of intrinsic defects that act as recombination centres. Another method to improve the properties of $FeVO_4$ is to partially substitute Fe by Bi, but the preparation of $Fe_{1-x}Bi_xVO_4$ requires strict

conditions to avoid the formation of secondary phases [141]. Concerning the properties of the metastable phases of $FeVO_4$, only $FeVO_4$-II has been reported to get better photocatalytic and gas sensing properties than $FeVO_4$-I. Such phenomenon has been already observed in the case of metastable VO_2(B) phase compared to VO_2(M), where photocatalysis runs better in the presence of VO_2(B).

Another interesting iron vanadate is $Fe_2V_4O_{13}$. It has a monoclinic structure which is composed of *[VO_4]* tetrahedra and *[Fe_2O_{10}]* double octahedra that are linked together through edge sharing, thus forming an unusual horseshoe-like chain structure [144, 145]. Since the structure is composed of channels and pores, $Fe_2V_4O_{13}$ is also an excellent candidate as cathode material for lithium ions batteries. Indeed, it can deliver a discharge capacity of about 154 $mA{\cdot}h{\cdot}g^{-1}$ between 1.5 and 4.0 V without significant loss upon 50 cycles [144]. However, the synthesis of pure $Fe_2V_4O_{13}$ is extremely difficult since $FeVO_4$ is always observed as a secondary phase. Concerning the electronic band structure of $Fe_2V_4O_{13}$, it is a n-type semiconductor with an energy bandgap of 2.3 eV *i.e.* in the visible range. The conduction band minimum and valence band maximum are at -0.5 eV and 1.7 eV, respectively [146]. Therefore, regarding these energetic positions, $Fe_2V_4O_{13}$ is a promising photocatalyst, especially for hydrogen production by water splitting, while the porous structure is an advantage for the photocatalytic degradation of pollutants due to higher specific surface area. On the other hand, the drawbacks of $Fe_2V_4O_{13}$ are its low efficiency in photocurrent production and photon-to-electron conversion with values of 16 $\mu A{\cdot}cm^{-2}$ at 1.23 V *vs.* SHE and 1.5% IPCE at 350 nm under 1.4 V, respectively [145].

The other iron vanadates are less investigated although they are promising. For example, FeV_3O_8 which has a monoclinic structure exhibit an energy bandgap of 2.2 eV, thus being a potential visible light-driven photocatalyst [147]. Another one is spinel FeV_2O_4. It has a cubic structure that belongs to the space group $Fd\bar{3}m$. The structure is composed of *[FeO_4]* tetrahedra and *[VO_6]* octahedra, and iron is in 8 tetrahedral sites while vanadium is in 16 octahedral sites [148]. FeV_2O_4 is a promising semiconductor with a yellow colour and it has direct and indirect energy bandgap at 1.9 eV and 2.6 eV, respectively [149]. Compared to Fe_2O_3 and V_2O_5, this intermediate oxide exhibits better electronic properties such as e^-/h^+ pairs separation and transport. In addition, FeV_2O_4 is also a good candidate for PEC

applications since it can produce 0.18 $mA \cdot cm^{-2}$ photocurrent density under UV-visible light at 1.2 V along with an IPCE of 22% at 320 nm [149].

4.2.3 Copper vanadates

Copper vanadates exhibit different structures and stoichiometries like, for instance, CuV_2O_6, $Cu_2V_2O_7$ and $Cu_3V_2O_8$. These ternary vanadium oxides are intermediate oxides in the system $CuO\text{-}V_2O_5$. The control of experimental conditions during the preparation of the copper vanadates is required to design the oxide with particular stoichiometry [61, 150]. The stoichiometric ratio copper/vanadium is the parameter which influences the structure and properties of copper vanadates. Initially, copper vanadates have attracted the interest of scientists due to their layered structure and their high capacity for lithiation, thus being promising cathode materials for LIBs. In addition, copper vanadates are semiconductors with interesting energy bandgap, thus being promising for photocatalytic applications [61].

The most investigated copper vanadate is $Cu_3V_2O_8$. This ternary vanadium oxide exhibits different phases where the $\gamma\text{-}Cu_3V_2O_8$ is the most stable phase with a monoclinic structure [61]. The structure is composed of *[VO_4]* tetrahedra, square-planar *[CuO_4]* and square-pyramidal *[CuO_5]* [151]. $\gamma\text{-}Cu_3V_2O_8$ is a n-type semiconductor with indirect and direct energy bandgap of 1.8 eV and 2.7 eV, respectively [120]. Concerning the electronic band structure, the VB is composed mainly of oxygen 2p-orbitals while the CB is composed of the 3d-orbitals of vanadium and copper. Therefore, the direct E_g has been identified as electronic transition between O 2p-orbitals and Cu 3d-orbitals while the indirect E_g is between O 2p and V 3d orbitals [152]. Concerning the potential applications of $\gamma\text{-}Cu_3V_2O_8$ in photochemical processes, further development is required since it cannot be used as efficient photocatalyst due to weak production of photocurrent and low value of IPCE with 62 $\mu A \cdot cm^{-2}$ at 1.23 V *vs.* SHE and 3% at 360 nm, respectively [152]. In addition, $\gamma\text{-}Cu_3V_2O_8$ exhibits a short diffusion length along with a small E_g, thus favouring e^-/h^+ pair recombination.

Another copper vanadate which is of high interest is $Cu_2V_2O_7$. It is a n-type semiconductor which has a monoclinic structure and an energy bandgap of 2.0 eV [153, 154]. $Cu_2V_2O_7$ has been already investigated as cathode materials for LIBs but also as a photocatalyst. However, like $Cu_3V_2O_8$, high recombination rate of the charge carriers leads to limited

efficiency in photochemical processes. Beside the low E_g, $Cu_2V_2O_7$ exhibit a photocurrent of about 100 µA·cm^{-2} at 1.23 V *vs.* SHE while the IPCE is only 4% at 400 nm [154]. Therefore, to increase the performance of copper vanadates, composites with a Z-scheme structure or a type-II heterojunction can be designed (Figure 13). Such composites exhibit high rate of e^-/h^+ pairs separation since the photogenerated electrons and holes are spatially separated and accumulated in the components [153].

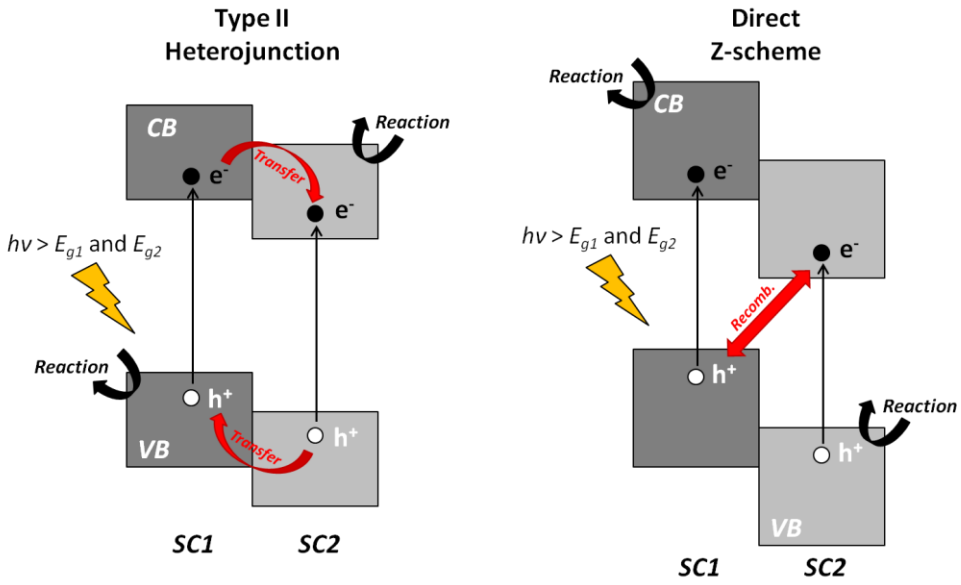

Figure 13. Electronic band structure: (left) type-II heterojunction and (right) direct Z-scheme [36].

5 Applications of vanadium-based oxides

5.1 Degradation of aqueous pollutants

5.1.1 V_2O_5

As mentioned above, V_2O_5 materials have already been investigated for electrochemical applications like LIBs. On the other hand, it is also a promising material for photocatalytic applications, especially the degradation of organic pollutants in water, since V_2O_5 has a suitable electronic band structure. Indeed, the VBM has been calculated up to 3.0 V, thus the redox for the generation of hydroxyl radicals ($E^o(HO^•/H_2O)$ = 2.8 V) is situated within the E_g. However, for the generation of superoxide anion radicals ($E^o(O_2/O_2^{•-})$ = -0.33 V), V_2O_5 is not

suitable since its CBM is less negative [155]. However, the surface defects *i.e.* the oxygen vacancies in the form of vanadium(IV) can lead to the production of $O_2^{\bullet-}$.

The properties of V_2O_5 and particularly its surface properties depend strongly on the preparation method of the photocatalyst, thus affecting their efficiency in the degradation f aqueous pollutants. Vanadium pentoxide can be synthesized in different forms (powders and supported layers) and morphologies (from 0D to 3D) by using a wide range of techniques such as sol-gel processes, solvothermal methods, solid-state reactions, electrochemical reactions or physical deposition techniques. Let's consider the wet chemical methods that involve the use of precursors. These techniques require an annealing step at about 500 °C during the preparation procedure to obtain crystalline V_2O_5 materials. For instance, thin V_2O_5 films can be deposited using the sol-gel method where vanadium triisopropoxide oxide precursor is employed in alcohol solvent [156, 157]. Films can be also prepared using hydrothermal methods where ammonium metavanadate (NH_4VO_3) or bulk V_2O_5 are used as precursors in water [158]. On the other hand, V_2O_5 powders can be also prepared by similar hydrothermal and sol-gel methods as well as by co-precipitation [159, 160]. In the latter case, the procedure often involves the NH_4VO_3 and HNO_3 as precursors [161]. Recently, various extra-drying processes (*e.g.* vaccum, freeze, oven) have shown beneficial effect during the preparation of V_2O_5 nanopowders since the aggregation of particles has been limited, thus increasing their specific surface area. Indeed, such extra-drying has led to nanoparticles with a size in the range from 30 to 40 nm and a specific surface area between 125 and 205 $m^2 \cdot g^{-1}$ [162]. Therefore, for all these techniques and by adjusting the experimental conditions (pH, structure directing substances, reducing/oxidizing agents, number of layers, precursor concentrations, etc.), materials with different morphologies can be obtained including hierarchical structure, nanorods, nanowires, etc. [156, 158].

For the degradation of organic pollutants in water, both films and powders have exhibited excellent efficiency through photochemical processes, especially photocatalysis [156, 157, 158, 159, 160, 161]. V_2O_5 nanowire films can degrade 98% of toluidine blue (an organic dye) after 50 min reaction under UV light [156]. Flower-like nanostructured films can remove up to 74% and 63% of methylene blue (an organic dye) under UV and visible light, respectively, after 200 min irradiation, and up to 50% mineralization extent (*i.e.* full degradation into CO_2, H_2O, and inorganic cations) can be observed [158]. Nanostructured powders can also

degrade efficiently organic dyes like rhodamine 6G, congo red and methyl orange with removal extents of 78%, 99% and 82%, respectively, after 180 min irradiation time under visible light [159, 160]. Under solar light, phenolic contaminants such as phenol, pyrocatechol, 2-chlorophenol, 2-nitrophenol and 2-aminophenol can be degraded in the presence of V_2O_5 with removal extents of 13%, 40%, 68%, 81% and 37%, respectively, along with the corresponding mineralization extents of 8%, 16%, 42%, 29% and 27% [161]. In addition, gaseous pollutants can be also efficiently degraded *via* V_2O_5 photocatalysis, such as 1,2-dichlobenzene which can be degraded under visible light after 7 h irradiation [157]. Furthermore, V_2O_5 nanopowders are also efficient antimicrobial agents that exhibit excellent removal extents of Escherichia coli and Staphylococcus aureus [159]. The reusability of V_2O_5 photocatalysts after successive runs is an important parameter to assess the reproducibility of the photocatalytic properties. In the case of V_2O_5, there is almost no change in the degradation extents of pollutants after repeated runs [159]. The excellent photocatalytic properties of V_2O_5 are mainly ascribed to large specific surface area and efficient incident light utilization [157, 158, 159, 160, 161]. In addition, the exposition of V_2O_5 to light irradiation induces the formation of surface defects (including the formation of vanadium(IV)), thus improving the lifetime of charge carriers by electron trapping phenomenon [161].

To assess the degradation mechanism of organic pollutants in the presence of V_2O_5 and light, the dark and blank experiments should be first performed *i.e.* direct photolysis (light without V_2O_5) and adsorption (V_2O_5 without light) of the aqueous pollutant. These 2 reference experiments lead to no significant degradation of any CEC, and it means that the potential degradation would be the result of photocatalysis [156]. Heterogeneous photocatalysis is a surface-dependent process which follows the Langmuir-Hinshelwood model. In other words, the degradation mechanism requires the adsorption of the target molecules (*e.g.* organic pollutants) at the surface of V_2O_5 where the photochemical reactions occur. Once adsorbed, the degradation of the organic pollutant is going through the attack by superoxide anion and hydroxyl radicals which are the primary ROS [157, 158, 159, 160, 161]. $HO^{\bullet}$ are formed by reaction between photogenerated holes and adsorbed water molecule (eqs. 4 and 5), but the involvement of $O_2^{\bullet-}$ is questionable since contradictory results are published in the literature. Indeed, the conduction band minimum is not thermodynamically suitable for the formation of $O_2^{\bullet-}$ while some scientists have claimed that superoxide anion radicals is transformed by a

cascade of reactions into hydroxyl radicals (eqs. 7-12) [157, 160, 161]. Therefore, to confirm the presence of these primary ROS, their identification by electron paramagnetic resonance (EPR) is required. Using EPR and DMPO (5,5-dimethyl-1-pyrroline N-oxide) as a probe molecule, signals of the DMPO-$HO^{\bullet}$ and DMPO-$O_2^{\bullet-}$ spin adducts with characteristics hyperfine structure have been identified, but the contribution of $O_2^{\bullet-}$ has been assessed as negligible [160].

Concerning the degradation pathways of organic pollutants, it depends on the type of the molecule. For aromatic compounds, the attack by $HO^{\bullet}$ leads to the ring opening and as the oxidation process goes, smaller molecule such as acetate and maleate are formed [157]. For organic dyes, it is often observed that the ROS trigger de-ethylation mechanism, thus forming smaller intermediates like benzoic acids which are further oxidized [159]. During the degradation of organic pollutants, the pH is a crucial parameter to consider. Indeed, the pH can affect the ionic form of the pollutant (which is related to its pK_a) but also the charge surface properties of the photocatalyst (with its isolelectric point), thus influencing the interactions pollutant/photocatalyst. In addition, the pH can also affect the generation of ROS since, for instance, the protonated form of the superoxide anion radical is predominant at low pH (eq. 7 and 8), thus allowing the formation of hydrogen peroxide (eq. 9) which is an important precursors of hydroxyl radicals (eqs. 10-12) [161].

To resume, V_2O_5 is a promising solar light driven photocatalyst for efficient water treatments from organic contaminants. However, further studies are required since, so far, most of them are focused on the removal of organic dyes. As model pollutants, organic dyes are not reliable to determine the intrinsic photocatalytic properties of a material because of the self-sensitization process *i.e.* the excited dyes can transfer electrons to the photocatalyst which subsequently can form ROS. Therefore, degradation of POPs and CECs using V_2O_5 is necessary to better assess the efficiency of this photocatalyst.

5.1.2 VO_2

As mentioned above, VO_2(M/R) has been thoroughly investigated for applications as smart windows due to its thermochromic properties. On the other hand, VO_2(B) has promising photocatalytic properties since it is a semiconductor material with an energy bandgap of

about 2.8-3.5 eV (according to the preparation procedure) [163, 164]. VO_2(B) has similar layered structure to V_2O_5, so their preparation procedure also shows some similarities. Indeed, using the sol-gel method, the same precursors can be used *i.e.* V_2O_5 powder which is dissolved in H_2O_2. The resulting aqueous sol-gel can be dried to form a powder or deposited in the form of film on silica or alumina substrate. It is worth noting that soda-lime glass substrate is not appropriate due to contamination from substrate by ion diffusion. Then, contrary to V_2O_5, the heat treatment should involve reducing conditions *e.g.* H_2/Ar atmosphere or high vacuum [165]. The reducing conditions imply the reduction of V_2O_5 into VO_2(B) via the mixed valence V_4O_9. Another preparation procedure is the solvothermal method where V_2O_5 powder is used as precursors, but in the case of VO_2(B), reducing agents are added to the system, like oxalic or citric acid [164, 166, 167, 168, 169].

The literature on VO_2(B) photocatalyst is relatively scarce, but it has been proven that its efficiency in the degradation of organic pollutants is better than that of V_2O_5 photocatalyst, especially for the removal of rhodamine B (an organic dye) under UVA light [163]. The superior photocatalytic properties of VO_2(B) over V_2O_5 has been ascribed to the surface defects (from preparation procedure which involves a reducing step) that lead to more oxygen vacancies, thus being beneficial for the e^-/h^+ pairs separation. Concerning the degradation mechanism of organic pollutants, the use of VO_2(B) photocatalysts involves the generation of primary ROS (*i.e.* $HO^\bullet$ and $O_2^{\bullet-}$) which have been identified as the main active species for the degradation and the mineralization of the pollutants [164]. On the other hand, there are more works on composite systems that are published especially based on VO_2(B) and VO_2(M) and the degradation mechanism proceeds similarly.

For example, VO_2(B)/CeO_2 photocatalysts in the form of nanoparticles exhibit high efficiency for the degradation of rhodamine B with a removal extent of 66% after 180 min UVA irradiation while it is only 29% for VO_2(B) [164]. The better efficiency of the composite is explained by a decrease of the E_g from 3.5 eV to 3.25 eV, thus allowing the utilization of larger portion of UVA light. In addition, CeO_2 can play the role of an electron trap that improves the e^-/h^+ pairs separation [164]. It is also plausible that CeO_2 can trigger Fenton-type reactions that enhance the production of ROS.

Another efficient composite is VO_2(M)/ZnO. In the form of hierarchical structure, it exhibits high specific surface area (70 $m^2 \cdot g^{-1}$) and an energy bandgap of about 2.7 eV. Compared to

VO_2(M), the SSA is increased by a factor 2 but the E_g is widened from 2.3 eV to 2.7 eV due to the presence of ZnO [167]. VO_2(M)/ZnO forms a type-II heterojunction where the photogenerated holes are accumulated in VO_2 and the photogenerated electrons are transferred to ZnO, thus limiting the e^-/h^+ pairs recombination. Such a configuration limits also the photo-corrosion of ZnO (eq. 25). Therefore, the composite exhibits a good photo-stability in solution, and it can be reused. The VO_2(M)/ZnO photocatalyst can degrade up to 80% rhodamine B under solar-like irradiation after 20 min, that is significantly better than the single components [167].

$$ZnO + 2h^+ \rightarrow Zn^{2+} + 1/2O_2 \qquad (25)$$

The VO_2(M)/TiO_2 composite is also interesting since it can combine different properties. Indeed, in the form of film deposited on glass, it can be used as photocatalyst, self-cleaning coating and thermochromic materials, thus being promising for smart window applications [166, 167, 169]. Such a composite can degrade completely methylene blue within 10 min under UV light and about 70% of rhodamine B after 2.5 h under simulated solar light. However, the excellent photocatalytic properties are ascribed to TiO_2, thus assuming a negligible contribution of VO_2(M) [166, 169].

To resume, vanadium dioxide and especially VO_2(B) is a photocatalyst for the degradation of organic pollutants in water. However, like V_2O_5, further studies are required by using a wider range of contaminants to better understand the degradation mechanism, the degradation pathway and thus, to assess the photocatalytic properties of this photocatalyst.

5.1.3 Mixed valence oxides

Among the mixed valence vanadium oxides that are used for photocatalytic applications, V_4O_9 and V_6O_{13} are the most investigated ones. Their use as photocatalysts is promising since V_2O_5 containing high number of electronic defects *i.e.* the presence of large amount of vanadium (IV) at the surface of V_2O_5 has exhibited excellent photocatalytic properties [170]. Therefore, by extension, binary vanadium oxides with mixed vanadium (V) and (IV) can have

a key role in the efficient separation of e^-/h^+ pairs, thus leading potentially to high efficiency for the photocatalytic degradation of organic pollutants in water [170, 171]. However, the literature of V_4O_9 and V_6O_{13} photocatalysts is limited although they appear better than V_2O_5 and VO_2 [172]. It worth noting that the synthesis of such mixed valence vanadium oxides required, like VO_2, reducing conditions since V_2O_5 or NH_4VO_3 are used as precursors.

For photocatalytic applications, V_6O_{13} is probably the most documented mixed valence vanadium oxides, especially in the form of composites [170, 171, 172]. Indeed, under visible light, V_6O_{13}/Al_2O_3 can degrade a wide range of pollutants including primary and secondary alcohols. For example, 3-hexanol is completely degraded after 24 h irradiation time while using VO_2 and V_2O_5, the degradation is negligible [172]. It is worth noting that the degradation of these alcohol is selective with about 70% of the alcohols is oxidized into aldehydes and ketones. V_6O_{13}/Al_2O_3 photocatalyst can also efficiently degrade saturated hydrocarbons, especially aromatics such as xylene and toluene [172]. VO_2/V_6O_{13} is also an efficient photocatalyst for the degradation of atrazine and methylene blue where, under visible light, atrazine is completely mineralized after 2 h and methylene blue can be degraded up to 75% after 1 h [171]. These excellent degradation extents under visible light are due to the high specific surface area (about 25 $m^2 \cdot g^{-1}$), the small energy bandgap (2.4 eV), but also to the efficient heterojunction between the components of the photocatalyst. In addition, V_6O_{13}/Al_2O_3 exhibits excellent reproducibility, thus enabling its reuse.

Another popular mixed valence vanadium oxide photocatalyst is V_4O_9 which has an energy bandgap of about 2.1 eV [173]. Although it is slightly less efficient than V_6O_{13}, it remains efficient for the degradation of organic pollutants in water. Indeed, V_4O_9 photocatalyst can degrade 45% of rhodamine B after 3 h under visible light. However, the photocatalytic properties of V_4O_9 are not often described in the literature due to several reasons: (i) like V_2O_5, it has a layered structure and an orthorhombic crystal structure, thus being hardly distinguishable compared to V_2O_5 which is much easier to prepare; and (ii) its photocatalytic properties are similar to those of V_2O_5 [173]. Consequently, it is plausible that V_4O_9 has been confused with V_2O_5.

Concerning the degradation mechanism of organic pollutants using these mixed valence vanadium oxides, the presence of oxygen vacancies (that are the result of the presence of both vanadium (IV) and (V) at the surface) increases the adsorption abilities of the

photocatalyst toward the pollutant [170]. The presence of mixed valence vanadium leads, as mentioned above, to better charge carrier separation, thus leading to enhanced production of ROS including hydroxyl radicals and superoxide anion radicals that are responsible of the mineralization of the organic pollutants into CO_2, H_2O and inorganic ions [171]. However, for V_4O_9, $O_2^{\bullet-}$ has been identified as the predominant reactive species for the degradation of organic pollutants [173]. In addition to the photocatalytic mechanism, removal by chemisorption has been also monitored. Indeed, such mechanism is based on the formation of V-O-C bond between the photocatalyst surface and the organic pollutant. Subsequently, the excitation of such a bond causes the elimination of proton in the alpha position, thus leading to the formation of by-products [172].

Here, again, further studies are required to understand but also to develop the photocatalytic applications using mixed valence vanadium oxides for the degradation of organic pollutants in water.

5.1.4 Bismuth vanadates

Among the ternary vanadium oxides, $BiVO_4$ is probably the most investigated one. It is mainly due to the presence of bismuth. As mentioned above, Bi broadens the utilization of light of the vanadium oxide in the visible region, thus $BiVO_4$ is a promising solar light-driven photocatalyst. In addition, $BiVO_4$ is environmentally friendly due to its non-toxicity and high stable, thus being a relevant photocatalyst for environmental purposes [135, 174]. The use of $BiVO_4$ photocatalysis is widely described in the literature. The efficiency in the degradation of organic pollutants using $BiVO_4$ differs from one work to another due to the various existing preparation procedures, thus leading to different morphological, surface and electronic properties [174, 175]. Also, different model pollutants and types of light are also used [9]. $BiVO_4$ can be prepared either in the form of powder or film. The latter *i.e.* supported material is beneficial for potential applications due to the ease of post-separation process.

Most of the literature on $BiVO_4$ as photocatalyst is devoted to the degradation of organic dyes. Although they are not considered as suitable model pollutants (due to photosensitization), the organic dyes remain environmentally relevant contaminants and they also provide an overview on the feasibility of the tested photocatalyst for the

degradation of organic pollutants. $BiVO_4$ with 1D and 2D morphology can degrade up to 93% of methylene blue and 86% of methyl orange after 60 and 150 min irradiation under visible light, respectively. The high specific surface area is one of the main reasons that explain these excellent degradation extents. Compared to bulk $BiVO_4$ (SSA = 0.5 $m^2 \cdot g^{-1}$), 1D and 2D $BiVO_4$ have SSA ranging from 5 to 45 $m^2 \cdot g^{-1}$ [174]. High SSA is associated with high number of active sites at the surface of the photocatalyst along with better adsorption properties. In addition, the bulk e^-/h^+ pairs recombination is limited in nanostructured materials due to shorter pathways for the charge carriers to reach the surface, thus enhancing their transfer at reactions interface. Other $BiVO_4$ morphologies can be designed like hierarchical structures. Such morphologies including dendritic, hollow sphere and olive-like $BiVO_4$ are efficient in the degradation of aqueous organic dyes (*e.g.* rhodamine B and methylene blue). Indeed, 80% degradation extents can be achieved after short irradiation times under visible light thank to high specific surface area (> 2 $m^2 \cdot g^{-1}$) [174]. However, most of the literature is devoted to the degradation of the initial organic dye molecule, and further studies on the mineralization extents and the degradation pathways are required to better assess the efficiency of $BiVO_4$. To this end, total organic carbon and mass spectrometry analyses appear to be appropriate techniques. For instance, although $BiVO_4$ can degrade completely methylene blue under visible light, only 65% is mineralized while the intermediation degradation by-products are composed of hydroxylated aromatics [9]. Similarly for rhodamine B, $BiVO_4$ can lead to only 40% mineralization extent after 100 h irradiation time under visible light [176]. In the latter case, removal of the chromophore and de-ethylation process have been identified as the main degradation pathways with the formation of ethylbenzene, xylene, etc., that are toxic intermediates. To get deeper insights into the efficiency along with the intrinsic photocatalytic properties of $BiVO_4$ photocatalysis, uncoloured persistent and/or emerging pollutant can be used as model pollutants since the contribution of self-sensitization is suppressed [9]. For instance, the degradation of pharmaceutical substances and endocrine disruptor compounds (EDCs) is often performed using photocatalysts. Indeed, $BiVO_4$ can degrade about 90% of ibuprofen and 65% of ciprofloxacin under UVA light [177, 178]. $BiVO_4$ photocatalyst also exhibits high efficiency in the degradation of EDCs including phenolic compounds (nonyl- and octyl-phenols) [179]. Beside aqueous pollutants, volatile organic contaminants (isopropyl alcohol, acetone, etc.) and gaseous pollutants (NO_x, etc.) can also be degraded *via* $BiVO_4$ photocatalysis [180, 181]. For example, N_2O which is a well-known

greenhouse gas from car pollution can be converted up to 25% by $BiVO_4$ after 12 h under visible light.

Concerning the degradation mechanism of organic pollutants using $BiVO_4$ photocatalyst, there are some contradictions in the literature. Although the preparation procedure of the photocatalyst can influence the position of the valence and conduction bands in the electronic band diagram, there is a misinterpretation of the results either from inadequately chosen analytical methods or by not considering the side processes (like self-sensitization). Therefore, from one work to another, the main reactive species that have been identified are either $HO^{\bullet}$, $O_2^{\bullet-}$ or even the photogenerated holes. It is worth noting that different methods exist to identify the ROS. Among them, the scavenging method, which consists of using a compound with significantly higher kinetic constant toward the target reactive species than the organic pollutant, is strongly sensitive to concentration of the scavengers, thus requiring calculations to avoid the quenching of the other reactive species. In other words, this method is not highly reliable, but it can help to draw the bases of a degradation mechanism. Other methods like EPR and fluorescence UV-visible spectroscopy are more accurate since it involves the use of a probe molecule which selectively react with the target reactive species, thus giving deeper insight into the degradation mechanism than the scavenging method. Using EPR, it has been proven that $BiVO_4$ photocatalyst cannot generate neither hydroxyl radicals nor superoxide anion radicals [182]. That is in accordance with the theoretical electronic band structure of monoclinic scheelite $BiVO_4$. Indeed, the conduction band minimum and valence band maximum are situated at 0 V and 2.4 V *vs.* SHE, respectively (Figure 14), thus the redox potentials for the formation of primary ROS *i.e.* $E^0(O_2/O_2^{\bullet-})$ and $E^0(OH^{\bullet}/H_2O)$ are not within the energy bandgap of $BiVO_4$ [9, 175, 182, 183]. Although the generation of primary ROS is not thermodynamically favoured, $HO^{\bullet}$ has been often identified in the degradation mechanism of some pollutants using $BiVO_4$ photocatalyst. Therefore, the question is: how is that possible? To answer this question, let's consider 2 possible side mechanisms.

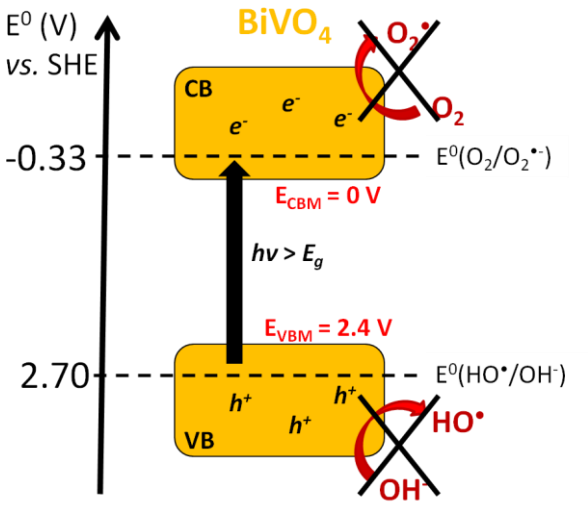

Figure 14. Energy diagram of the band structure of $BiVO_4$ photocatalyst [36].

The first one is related to the effect of pH. Indeed, the electronic band structure of $BiVO_4$ depends somehow on the preparation procedure of the photocatalyst, but the pH can also affect the positions of VBM and CBM. Indeed, in Figure 14, the electronic band structure is calculated for pH = 0 (*vs.* SHE), but for the degradation of organic pollutants, the pH is usually about circumneutral, thus leading to a shift of the band structure towards negative energies. Consequently, the generation of $O_2^{\bullet-}$ becomes thermodynamically feasible since $E^o(O_2/O_2^{\bullet-})$ is then situated within E_g of $BiVO_4$. In addition, the superoxide anion radical can be converted into $HO^\bullet$ *via* H_2O_2 by a cascade of photocatalytic, acido-basic and redox reactions (eqs. 7-12) [176, 177, 184].

A second side mechanism is the self-sensitization of the photocatalyst by organic dyes. Under light, the organic dye is absorbing a photon that leads to an excited state (eq. 26). The excited electron can be transferred to the CB of $BiVO_4$ (eq. 27), thus enabling reaction with oxygen to form $O_2^{\bullet-}$ [176]. Therefore, this self-sensitization process can generate ROS independently to the photocatalytic activation of $BiVO_4$. In the presence of an organic dye, the intrinsic photocatalytic properties of $BiVO_4$ cannot be determined.

$$\text{Dye} + h\nu \longrightarrow \text{Dye}^* \qquad (26)$$

$$BiVO_4 + \text{Dye}^* \longrightarrow \text{Dye}^{\bullet+} + BiVO_4(e^-) \qquad (27)$$

Other bismuth vanadates like $Bi_4V_2O_{11}$ and $Bi_8V_2O_{17}$ photocatalysts can be used for the degradation of organic pollutants in water [185, 186]. The preparation procedure for these visible light-driven photocatalysts is similar to that of $BiVO_4$ but using different stoichiometric ratio between the precursors. However, such mixed valence bismuth vanadate cannot be prepared as pure since $BiVO_4$ is often present as an impurity. For the degradation of organic pollutants, $BiVO_4/Bi_4V_2O_{11}$ can degrade 95% of sulfamethazine under visible light along with a mineralization extent of 50% [185]. In addition, the superoxide anion radicals have been identified as the main reactive species.

To resume, bismuth vanadates and especially $BiVO_4$ appears highly promising photocatalysts for the degradation of organic pollutants in water, but further studies are required to clear out the uncertainties about their photocatalytic efficiency.

5.1.5 Iron vanadates

Iron vanadates are interesting materials for the degradation of organic pollutants due to several reasons: (i) they are semiconductor photocatalysts but also (ii) materials active in Fenton-based processes due to the presence of chemical elements that are active in Fenton, Fenton-like and photo-Fenton processes. Among the iron vanadates, $FeVO_4$ is the most investigated one. It has E_g of about 2.1 eV with CBM and VBM at -0.6 eV and 1.5 eV, respectively, thus being a photocatalyst potentially active under visible light [143]. $FeVO_4$ can be prepared using wet chemical methods where, for instance, precursors based on iron (III) and metavanadate salts are involved along with structure directing agents to design particular morphologies [117, 143]. Therefore, according to the experimental conditions of the preparation procedure, various morphologies can be prepared, thus leading to $FeVO_4$ with small variation in the electronic band structures. Indeed, nanostructured $FeVO_4$ exhibits higher E_g than the bulk oxides, while the specific surface area can vary from 15 to 30 $m^2 \cdot g^{-1}$ [117, 143, 187, 188, 189].

Concerning the degradation of organic pollutants, $FeVO_4$ photocatalyst can degrade 90% of rhodamine B and 50% of phenol red after 300 min and 120 min irradiation time under UVA

light, respectively [143, 187, 189]. Under visible light, the degradation efficiency decreases. Indeed, for the degradation of rhodamine B, the removal and mineralization extents reach 70% and 10M after 5 h irradiation [137, 143, 188, 189]. However, since iron is present in the material, Fenton-based processes can be triggered in the presence of hydrogen peroxide, and the degradation of rhodamine B can be completed under visible light [189]. Compared to classical heterogeneous Fenton-based systems *i.e.* hematite (α-Fe_2O_3), magnetite (Fe_3O_4) and goethite (γ-FeOOH), $FeVO_4$ exhibits enhanced efficiency for the degradation of organic pollutants due to more efficient activation of H_2O_2 into $HO^\bullet$. For example, 90% degradation extent of methyl orange is obtained after 1 h irradiation time using $FeVO_4$ [139]. In addition, $FeVO_4$ can also activate peroxymonosulfate (HSO_5^-) into sulphate radicals ($SO_4^{\bullet-}$), thus leading to the degradation of 96% of sulfamethoxazole after 1 h under visible light [190].

Concerning the degradation mechanism, both photocatalytic and Fenton-based processes are involved. For photocatalysis, the electronic band structure of $FeVO_4$ allows the formation of superoxide anion radicals since $E^0(O_2^{\bullet-}/O_2)$ is situated within the energy bandgap. Hydroxyl radicals cannot be produced because $E^0(H_2O/HO^\bullet)$ is more positive than the valence band maximum [117]. However, $HO^\bullet$ can be generated by self-sensitization of $FeVO_4$ in the case an organic dye is aimed to be degraded (eqs. 26 and 27) or by conversion of $O_2^{\bullet-}$ according to eqs. 7-12. For Fenton-based processes, the activation of H_2O_2 by $FeVO_4$ follows a 2-way reaction scheme [139, 191]. H_2O_2 is first activated into hydroperoxyl radical ($HO_2^\bullet$) by Fenton-like reaction (eqs. 14 and 29) since iron(III) and vanadium(V) are present at the surface of $FeVO_4$. Subsequently, iron(II) and vanadium(IV) is formed and they can activate H_2O_2 into $HO^\bullet$ through classical Fenton reactions (eqs. 13 and 28). In addition, photo-Fenton reaction using iron(III) is also plausible (eq. 15). However, these Fenton-based processes are still the matter of intense discussion since the kinetic constants of Fenton-like reactions are much lower than those for classical Fenton ones, thus cycles between Fe(III)-Fe(II) and V(V)-V(IV) are slow. In addition, heterogeneous Fenton-based processes have not been yet resolved since it is still not clear whether reactions occur at the surface of the material or in a space close to it (*i.e.* due to potential Fe and/or V leaching) [139, 190]. Nevertheless, $HO^\bullet$ has been identified as the main reactive species during the degradation of organic pollutants using $FeVO_4$ and H_2O_2 under light [139, 190]. By using HSO_5^- instead of H_2O_2, sulphate radicals, that have similar oxidation power as $HO^\bullet$, can be produced from iron(II) and vanadium(IV)

(eq. 30). In addition, $SO_4^{\bullet-}$ can be converted into hydroxyl radicals in the presence of hydroxide anions (eq. 31).

$$V^{4+} + H_2O_2 \rightarrow V^{5+} + OH^- + HO^{\bullet} \quad (28)$$

$$V^{5+} + H_2O_2 \rightarrow V^{4+} + H^+ + HOO^{\bullet} \quad (29)$$

$$Fe^{2+}/V^{4+} + HSO_5^- \rightarrow SO_4^{\bullet-} + OH^- + Fe^{3+}/V^{5+} \quad (30)$$

$$SO_4^{\bullet-} + OH^- \rightarrow SO_4^{2-} + HO^{\bullet} \quad (31)$$

To improve the efficiency of $FeVO_4$ in photochemical processes for the degradation of organic pollutants, composite can be designed. $ZnO/FeVO_4$ material in the presence of H_2O_2 can trigger simultaneously photocatalytic and Fenton-based processes under UVA light, thus leading to 93% degradation extent of sodium dodecyl sulphate after only 1 h irradiation time [192]. Similarly, $FeVO_4/CeO_2$ can remove 94% of 4-nitrophenol after 1 h under visible light [191]. Other composites like $FeVO_4/V_2O_5$, $FeVO_4/BiVO_4$ and $FeVO_4/Fe_2O_3$ have exhibited efficient degradation extents for the degradation of organic dyes including rhodamine B, phenol red, methyl violet and methylene blue [118, 193, 194].

Concerning the degradation mechanism of organic pollutants using $FeVO_4$ composites, most of the literature discussed only the photocatalytic process, especially the type of heterojunctions that limit the e^-/h^+ pairs separation. Indeed, direct Z-scheme or type-II heterojunction (Figure 13) helps to increase the lifetime of charge carriers (by separated accumulatio of e^- end h^+) but also the better utilization of light (by a decrease of E_g). Therefore, the choice of the components is crucial in $FeVO_4$ composites. For example, a type-II heterojunction is $FeVO_4/CeO_2$ where the CBM of $FeVO_4$ and CeO_2 are at -0.45 eV and -0.32 eV, respectively, and their VBM are at 1.55 eV and 2.45 eV, respectively [191]. Under suitable light, the photogenerated e^- are accumulated in the CB of CeO_2 while h^+ are transferred in the VB of $FeVO_4$, but only superoxide anion radicals can be generated. In the case $FeVO_4$ is decorated by CeO_2, the latter rather acts as an electron scavenger. In addition, $FeVO_4/CeO_2$ can trigger Fenton-based processes since cerium is an element that can activate H_2O_2 into $HO^{\bullet}$ (eqs. 18 and 19) [139, 191]. Beside the type-II heterojunction, an example of direct Z-

scheme is $FeVO_4/Fe_2O_3$. The principle of these 2 different configurations is the same: to avoid e^-/h^+ pairs recombination. In direct Z-scheme, the energetic position of the CBM of the first component is close to that of the VBM of the second component (Figure 13). Therefore, for $FeVO_4/Fe_2O_3$ under suitable light, the photogenerated e^- and h^+ that are present in the CB of $FeVO_4$ and VB of Fe_2O_3 can react rapidly to generate primary ROS since the e^- and h^+ in the remaining bands combine due to very close energies (Figure 15). Consequently, regarding the electronic band structure of $FeVO_4/Fe_2O_3$, a direct Z-scheme would allow the generation of primary ROS while a type-II heterojunction cannot lead to their formation (Figure 15). In the literature, hydroxyl radicals have been identified in the degradation of organic pollutant using $FeVO_4/Fe_2O_3$, thus confirming that such a composite has a direct Z-scheme structure [194]. Usually, whatever the configuration of the $FeVO_4$ composite, most of them exhibit improved efficiencies for the degradation of organic pollutants from 10% to 80% (according to the experimental conditions) compared to the single components [118, 193, 194].

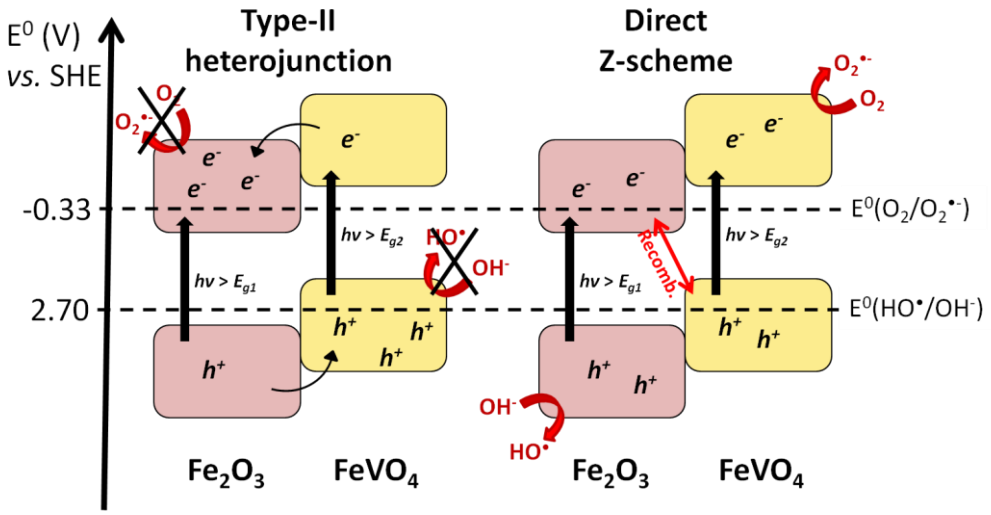

Figure 15. The electronic band structures of $FeVO_4/Fe_2O_3$ composite either in a type-II heterojunction or a direct Z-scheme configuration, along with the generation of primary ROS [36].

On the other hand, other iron vanadates are also promising photocatalysts for the degradation of organic pollutants. It is the case $Fe_2V_4O_{13}$ which is a visible light-driven photocatalyst with an energy bandgap in the range 2.2-2.8 eV [195, 196]. $Fe_2V_4O_{13}$ has CBM and VBM at -2.05 eV and 0.15 eV, respectively [196]. Therefore, the degradation of organic pollutants only proceeds by attack of superoxide anion radicals, thus being relatively

inefficient for complete mineralization. However, since $Fe_2V_4O_{13}$ exhibits strong reductive properties (CBM < 2 eV), it can be used to remove the highly carcinogenic Cr(VI). Indeed, the photocatalytic reduction of Cr(VI) to Cr(III) using $Fe_2V_4O_{13}$ can achieve a conversion extent of 98% [195]. To degrade efficiently organic pollutants, $Fe_2V_4O_{13}$ is used in the form of composites. For instance, $Fe_2V_4O_{13}$/ZnO is a type-II heterojunction where the electronic band structure can allow only the production of $O_2^{\bullet-}$ under suitable light. Although the generation of $HO^{\bullet}$ is still not thermodynamically feasible, $Fe_2V_4O_{13}$/ZnO can degrade 90% of methyl orange under solar light, that is much more than pristine $Fe_2V_4O_{13}$ [196]. However, mineralization extent remains low, thus highlighting the need of further research to design more efficient $Fe_2V_4O_{13}$ composite, probably using a component that could form a direct Z-scheme for the production of $HO^{\bullet}$. Although $Fe_2V_4O_{13}$ is not an ideal candidate for photocatalysis, it can be used in multi-Fenton processes like $FeVO_4$. In the presence of H_2O_2, a two-way reaction scheme occurs where ROS are produced (eqs. 13, 14, 28 and 29). $Fe_2V_4O_{13}$ is an efficient multi-Fenton catalyst since it can degrade more than 90% of methyl orange associated with a mineralization extent of 40% [197]. In addition, $Fe_2V_4O_{13}$ has exhibited better efficiency for the degradation of organic pollutants using Fenton-based processes than other systems ($FeVO_4$/V_2O_5, Fe_2O_3/V_2O_5, etc.) at similar experimental conditions.

Another interesting iron vanadate is FeV_3O_8 which exhibits an energy bandgap at 2.23 eV, thus being promising for visible light-driven photocatalysis. Such a photocatalyst can remove up to 92% of methyl orange after only 30 min under visible light [147]. The main reactive species that have been identified superoxide anion radicals and hydroxyl radicals. However, like all the vanadium-based oxides, further studies are required to clearly elucidate the photocatalytic degradation mechanism of organic pollutants.

5.1.6 Other vanadium-based oxides

Many other ternary vanadium oxides in either pure or composite materials have been used in photochemical processes for the degradation of organic pollutants. Some of them along with their optical properties and their degradation efficiencies are summarized in Table 1. Although these vanadium-based oxides are promising photocatalysts, their use for the degradation of organic pollutants is far less documented than binary vanadium oxides, and

bismuth and iron vanadates. Therefore, further research is necessary to develop their potential use in photochemical processes including photocatalytic and Fenton-based processes.

Table 1. Overview of different metal vanadates used in photochemical processes for the degradation of organic pollutants

System	E_g (eV)	Pollutant	Incident irradiation	Degradation extent	Ref.
$Cu_3V_2O_8$	2.05-2.10	Methyl orange	UVA light	78% after 120 min	[120]
VO_2/Ag_3VO_4	-	Rhodamine B	Solar light	73% after 90 min	[168]
$Mn(VO_3)_2$	3.05	Methyl orange	UVA light	84% after 80 min	[198]
$Mn_2V_2O_7$	2.79	Methylene blue	Solar light	90% after 4 h	[199]
$AgVO_3/BiVO_4$	2.32-2.43	Rhodamine B	Visible light	93% after 120 min	[200]
$CeO_2/CeVO_4/V_2O_5$	2.26-2.93	Methylene blue	Visible light	93% after 4 h (189 µmol of produced H_2)	[201]
$Ag_4V_2O_7/BiVO_4$	2.36-2.41	Methylene blue and NO	Visible light	98% for MB and 53% for NO after 30 min	[202]
$Cu_3V_2O_7(OH)_2{\cdot}2H_2O$	2.1	Methylene blue	Visible light	~90% after 150 min	[203]
$Cu_3V_2O_8$	-	Methyl orange	UVA light	72% after 100 min	[204]
$Cu_2V_2O_7 (+H_2O_2)$	2.17	Evans blue	UVA light	77% after 120 min	[205]

5.2 Production of hydrogen

TiO_2 has been the first photocatalyst to be investigated for the production of hydrogen by water splitting using a photoelectrochemical cell [73]. This discovery opens the door for the development of other photocatalysts which can split water molecules under visible light since TiO_2 is a UV light-driven photocatalyst. Although Fe_2O_3, WO_3 and CdS are visible light-driven photocatalysts, these candidates are not viable for hydrogen production by water splitting due to either inappropriate electronic band structure, low photostability, high recombination rate or high toxicity [69, 70]. Therefore, the choice of vanadium-based oxides appears obvious because many of them have a value of E_g in the visible region that also enclose the redox potential for water splitting *i.e.* water reduction (H_2 production) and water oxidation (O_2 production) [206, 207].

Due to these promising properties, some binary vanadium oxides including V_2O_5, VO_2(M), VO_2(B) and V_6O_{13} have been investigated for hydrogen production by water splitting without using a PEC cell *i.e.* without any voltage. Under visible light, these binary vanadium oxides can produce up to 35 µmol of H_2 after 12 h irradiation time [206]. To increase the production rate of hydrogen, sacrificial agent can be used to avoid the production of oxygen but also to increase the e^-/h^+ pairs separation. For instance, an alcohol can be used to scavenge the photogenerated holes, thus avoiding the production of oxygen ($k_{h+/alcohol} >> k_{h+/water}$) and supporting the electron transfer to the CB of the photocatalyst. Under visible light, supported VO_2 nanorods can produce 800 mmol·m^{-2}·h^{-1} of H_2 in the presence of ethanol and V_2O_5 is able to generate about 9 mm^3·h^{-1} of H_2 in the presence of methanol [208, 209]. Beside the use of alcohol as sacrificial agent to improve the hydrogen production by water splitting (Figure 16A), photo-sensitization process using, for instance, Eosin Y dye can be also used to increase the population of electrons in the CB of the photocatalyst (Figure 16B). By this mean, the production of H_2 by H_2O splitting using V_2O_5 can reach almost 20 mm^3·h^{-1} [209].

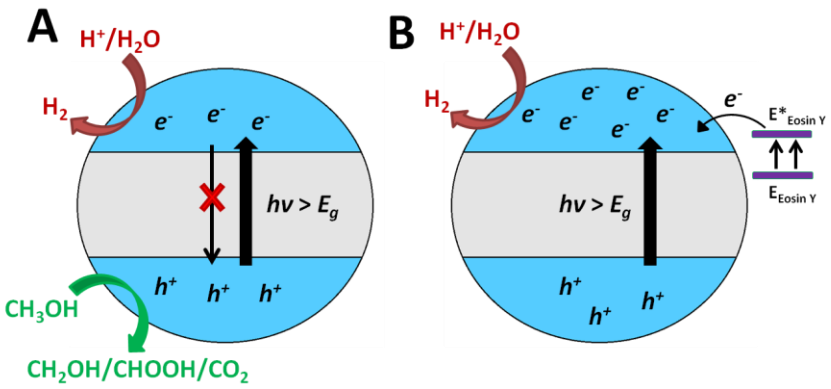

Figure 16. Improvement of hydrogen production using semiconductor photocatalyst by (A) sacrificial agent method (here, methanol) and (B) by photo-sensitization (here, Eosin Y dye) [36].

However, using pure vanadium-based oxide photocatalyst, the production rate of hydrogen remains low due to important e^-/h^+ pairs recombination and limited incident photon-to-electron efficiency [210, 211]. In addition, some vanadium-based oxides like $BiVO_4$ have a CBM near 0 V *vs.* SHE, thus the production of hydrogen by water splitting cannot occur due to overpotential losses. Furthermore, there are kinetic issues related to the number of available electrons from which 2 of them are required to form 1 hydrogen molecule. To

overcome these drawbacks, different strategies exist. One of them is the modification of the photocatalyst. Indeed, the use of co-catalyst at the surface of the photocatalyst can decrease the activation energy of water splitting to enhance the hydrogen production and also play the role of electron scavenger to increase the e^-/h^+ pairs separation. Another strategy is the design of composite photocatalyst with a type-II heterojunction or a direct Z-scheme configuration. In this case, under visible light, $FeVO_4$/CdS can produce 400 µM of H_2 by H_2O splitting after 5 hours under visible light and $BiVO_4$/CdS exhibits a hydrogen production rate of 0.57 $mmol \cdot h^{-1}$ [211, 212]. But the most efficient strategies is, by far, the use of an electrical bias in a PEC system where the photocatalyst is deposited as a photoelectrode. The principle of a PEC system is to enforce the motion of photogenerated electrons oppositely to that of the photogenerated holes, so the no recombination between e^- and h^+ occurs. In addition, the PEC cell can be composed of 2 compartments separated by ion-transfer membrane, so H_2 and O_2 evolve separately without any risk of water recombination nor even explosion. One of the most investigated vanadium-based oxides in PEC system is $BiVO_4$ photocatalyst which is used as a photoanode [207, 213, 214]. $BiVO_4$ exhibits excellent photocurrent under simulated solar light with values ranging from 6.2 to 7.5 $mA \cdot cm^{-2}$ (according to the applied voltage and the electrolyte), and it possesses also a highly positive VBM (2.4 V *vs.* SHE), thus the photogenerated holes are efficiently used in water oxidation [129]. In other words, the photogenerated electrons can be efficiently used in water reduction. Indeed, $BiVO_4$ photoanode can produce up to 2.5 $\mu mol \cdot min^{-1}$ of H_2 under simulated solar light at 1.4 V *vs.* Ag/AgCl [215]. Although such a production rate is relatively high, it could be enhanced by using composite photocatalysts since $BiVO_4$ is known for its poor electron mobility and short hole diffusion length [213]. For example, $BiVO_4$/$FeVO_4$ photoanode exhibits higher photocurrent density than the single components [216]. It is attributed to the accumulation of photogenerated electron in the CB of $BiVO_4$ which is at the contact of the electrode while the photogenerated holes are accumulated in the VB of $FeVO_4$ which is in contact with the reaction medium (Figure 17). Such a type-II heterojunction allows efficient transport of the electron to the cathode where the reduction reactions for the production of hydrogen occur. Beside the effect of the electronic band structure on the production rate of hydrogen by water splitting, other factors including the specific surface area, exposed crystal facets, and morphology have to be considered to optimize the H_2 generation [217, 218].

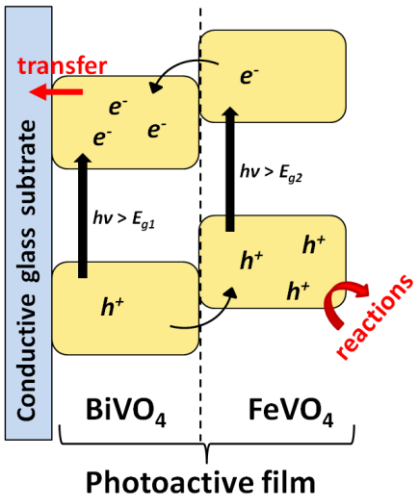

Figure 17. Electronic band structure of $BiVO_4/FeVO_4$ photoanode where $BiVO_4$ is in contact with the electrode. This type-II heterojunction exhibits efficient e^-/h^+ pairs separation [36].

6 Literature

[1] E. Azenha, A. Romeiro and M. Sarakha, "Photodegradation of pesticides and photocatalysis in the treatment of water and waste," in *Applied Photochemistry*, Dordrecht, Netherlands, Springer, 2013, pp. 247-266.

[2] U. I. Gaya, Heterogeneous photocatalysis using inorganic semiconductor solids, Dordrecht, Netherlands: Springer, 2014.

[3] L. Hinojosa-Reyes, J. L. Guzman-Mar and M. Villanueva-Rodriguez, "Semiconductormaterials for photocatalytic oxidation of organic pollutants in wastewater," in *Photocatalytic semiconductors*, Cham, Switzerland, Springer, 2015, pp. 187-228.

[4] D. G. J. Larsson, "Pollution from drug manufacturing: review and perspectives," *Philos. T. Roy. Soc. B*, vol. 369, pp. 71-78, 2014.

[5] S. Sauve, "Desrosiers, M. A review of what is an emerging contaminant," *Chem. Cent. J.* , vol. 8, pp. 15-21, 2014.

[6] T. Deblonde, C. Cossu-Leguille and P. Hartemann, "Emerging pollutants in wastewater: A review of the literature," *Int. J. Hyg. and Envir. Heal.*, vol. 214, pp. 442-448, 2011.

[7] N. Bolong, A. F. Ismail, M. R. Salim and T. Matsuura, "A review of the effects of emerging contaminants in wastewater and options for their removal," *Desalination,* vol. 239, pp. 229-246, 2009.

[8] B. Petrie, R. Barden and B. Kasprzyk-Hordern, "A review on emerging contaminants in watewaters and the environment: Current knowledge, understudied areas and recommendations for future monitoring," *Water Res.,* vol. 72, pp. 3-27, 2015.

[9] O. Monfort and G. Plesch, "Bismuth vanadate-based semiconductor photocatalysts: a short critical review on the efficiency and the mechanism of photodegradation of organic pollutants," *Environ Sci Pollut Res.,* vol. 25, pp. 19362-19379, 2018.

[10] H. Baharum, W. C. Chu, S. S. Teo, K. Y. Ng, R. A. Rahim and C. L. Ho, "Molecular cloning, homology modeling and site-directed mutagenesis of vanadium-dependent bromoperoxidase (GcVBPO1) from Gracilaria changii (Rhodophyta)," *Phytochemistry,* vol. 92, pp. 49-59, 2013.

[11] M. Liu, B. Su, Y. Tang, X. Jiang and A. Yu, "Recent Advances in Nanostructured Vanadium Oxides and Composites for Energy Conversion," *Adv. Energy Mater.,* vol. 7, p. 1700885, 2017.

[12] M. E. Weeks, "The Discovery of the Elements. VII. Columbium, Tantalum, and Vanadium," *J. Chem. Educ.,* vol. 9, no. 5, pp. 863-884, 1932.

[13] J. P. Gustafsson, "Vanadium geochemistry in the biogeosphere speciation, solid-solution interactions, and ecotoxicity," *Appl. Geochem.,* vol. 102, pp. 1-25, 2019.

[14] N. G. Safstrom, "Sur Le Vanadium, Métal Nouveau, Trouvé Dans Du Fer En Barres De Eckersholm, Forge Qui Tire Sa Mine De Taberg, Dans Le Smaland," *Ann. Chim. Phys.,* vol. 46, pp. 105-111, 1831.

[15] D. C. Adriano, Trace Elements in the Terrestrial Environment, New York, USA: Springer-Verlag, 1986.

[16] R. R. Moskalyk and A. M. Alfanti, "Processing of vanadium: a review," *Miner. Eng.,* vol. 16, pp. 793-805, 2003.

[17] E. F. Baroch, "Vanadium and vanadium alloys," in *Kirk-Othmer Encyclopedia of Chemical Technology*, New York, USA, Wiley, 2013, pp. 1-18.

[18] D. Rehder, "The potentiality of vanadium in medicinal applications," *Future Med. Chem.* , vol. 1823, p. 2012, 2012.

[19] J. Korbecki, I. Baranowska-Bosiacka, I. Gutowska and D. Chlubek, "Biochemical and medical importance of vanadium compounds," *Acta Biochim. Pol.,* vol. 59, p. 195, 2012.

[20] D. G. Barceloux, "Vanadium," *J. Toxicol. Clin. Toxicol.* , vol. 37, pp. 265-278, 1999.

[21] D. Rehder, "Vanadium. Its role for humans," *Met. Ions Life Sci.,* vol. 13, pp. 139-169, 2013.

[22] M. T. Wright and K. Belitz, "Factors controlling the regional distribution of vanadium in groundwater," *Ground Water,* vol. 48, pp. 515-525, 2010.

[23] V. B. Vouk and W. T. Piver, "Metallic elements in fossil fuel combustion products," *Environ. Health Perspect.,* vol. 47, pp. 2111-2225, 1983.

[24] P. Miramand and S. W. Fowler, "Bioaccumulation and transfer of vanadium in marine organisms," in *Vanadium in the Environment: Part 1. Chemistry and Biochemistry*, New York, USA, Wiley, 1998, pp. 167-169.

[25] D. Rehder, "The bioinorganic chemistry of vanadium," *Angew. Chem. Int. Ed. Engl.,* vol. 30, pp. 148-167, 1991.

[26] G. R. Willsky, L. H. Chi, M. Godzala, P. J. Kostyniak, J. J. Smee, A. M. Trujillo, J. A. Alfano, W. J. Ding, Z. H. Hu and D. C. Crans, "Anti-diabetic effects of a series of vanadium dipicolinate complexes in rats with streptozotocin-induced diabetes," *Coord. Chem. Rev.,* vol. 255, pp. 2258-2269, 2011.

[27] T. Kiss, E. Kiss, E. Garribba and H. Sakurai, "Speciation of insulin-mimetic VO(IV)-containing drugs in blood serum," *J. Inorg. Biochem.* , vol. 80, pp. 65-73, 2000.

[28] T. V. Hansen, J. Aaseth and J. Alexander, "The effect of chelating agents on vanadium distribution in the rat body and on uptake by human erythrocytes," *Arch. Toxicol.* , vol. 50, pp. 195-202, 1982.

[29] J. C. Pessoa, S. Etcheverry and D. Gambino, "Vanadium compounds in medicine," *Coordin. Chem. Rev.* , Vols. 301-302, pp. 24-48, 2005.

[30] K. Kanamori and K. Tsuge, "Inorganic Chemistry of Vanadium," in *Vanadium Biochemical and Molecular Biological Approaches*, Dordrecht, Netherlands, Springer, 2012, pp. 3-31.

[31] B. Mukherjee, B. Patra, S. Mahapatra, P. Banerjee, A. Tiwari and M. Chatterjee, "Vanadium - an element of atypical biological significance," *Toxicol. Lett.,* vol. 150, pp. 135-143, 2004.

[32] M. Almeida, S. Filipe, M. Humanes, M. F. Maia, R. Melo, N. Severino, J. A. L. Silva, J. J. R. F. d. Silva and R. Wever, "Vanadium haloperoxidases from brown algae of the Laminariaceae family," *Photochemistry,* vol. 57, pp. 633-642, 2001.

[33] A. S. Menon, M. Rau, T. Ramasarma and F. L. Crane, "Vanadate inhibits mevalonate synthesis and activates NADH oxidation in microsomes," *FEBS Lett.* , vol. 114, pp. 139-141, 1980.

[34] M. H. Golden and B. E. Golden, "Trace Elements: Potential Importance in Human Nutrition with Particular Reference to Zinc and Vanadium," *Brit. Med. Bull.* , vol. 37, pp. 3731-3736, 1981.

[35] A. R. Byrne and L. Kosta, "Vanadium in foods and in human body fluids and tissues," *Sci. Total Environ.* , vol. 10, no. 1, pp. 17-30, 1978.

[36] O. Monfort and P. Petriskova, "Binary and Ternary Oxides: General Overview, Physical Properties, and Photochemical Processes for Environmental Applications," *Processes,* vol. 9, p. 214, 2021.

[37] R. Ray, M. Basu, B. Ghosh, K. Samanta and M. Chatterjee, "Vanadium, a Versatile Biochemical Effector in Chemical Rat Mammary Carcinogenesis," *Nutr. Cancer.,* vol. 51, pp. 184-196, 2005.

[38] R. S. Ray, B. Rana, B. Swami, V. Venu and M. Chatterjee, "Vanadium mediated apoptosis and cell cycle arrest in MCF7 cell line," *Chem.-Biol. Interact.* , vol. 163, pp. 239-247, 2006.

[39] R. R. Langeslay, D. M. Kaphan, C. L. Marshall, P. C. Stair, A. P. Sattelberger and M. Delferro, "Catalytic Applications of Vanadium: A Mechanistic Perspective," *Chem. Rev.,* vol. 119, pp. 2128-2191, 2019.

[40] F. A. Cotton, G. Wilkinson, C. A. Murillo and M. Bochmann, Advanced Inorganic Chemistry, New York, USA: Wiley, 1999.

[41] Y. Ma, Y. Dai, M. Guo, C. Niu, Y. Zhu and B. Huang, "Evidence of the existence of magnetism in pristine VX2 monolayers (X = S, Se) and their strain-induced tunable magnetic properties," *ACS Nano,* vol. 6, pp. 1695-1701, 2012.

[42] J. Chmiola, C. Largeot, P. L. Taberna, P. Simon and Y. Gogotsi, "Monolithic Carbide-Derived Carbon Films for Micro-Supercapacitors," *Science,* vol. 328, p. 480, 2010.

[43] J. R. Miller, R. A. Outlaw and B. C. Holloway, "Graphene Double-Layer Capacitor with ac Line-Filtering Performance," *Science,* vol. 329, p. 1637, 2010.

[44] S. Bae, H. Kim, Y. Lee, X. Xu, J. S. Park, Y. Zheng, J. Balakrishnan, T. Lei, R. H. Kim, Y. I. Song, Y. J. Kim, K. S. Kim, B. Ozyilmaz, J. H. Ahn, B. H. Hong and S. Lijima, "Roll-to-roll production of 30-inch graphene films for transparent electrodes," *Nat. Nanotechnol.,* vol. 5, p. 574, 2010.

[45] C. Lamsal and N. M. Ravindra, "Vanadium Oxides: Synthesis, Properties, and Applications," in *Semiconductors*, Cham, Switzerland, Springer Nature, 2019, pp. 127-218.

[46] J. C. Parker, U. W. Geiser, D. J. Lam, Y. Xu and W. Y. Ching, "Optical properties of the vanadium oxides VO2 and V2O5," *J. Am. Ceram. Soc.* , vol. 73, pp. 3206-3208, 1990.

[47] D. Kucharczyk and T. Niklewski, "Accurate X-ray determination of the lattice parameters and the thermal expansion coefficients of VO2 near the transition temperature," *J. Appl. Cryst.* , vol. 12, pp. 370-373, 1979.

[48] H. Jerominek, F. Picard and D. Vincent, "Vanadium oxide films for optical switching and detection," *Opt. Eng.,* vol. 32, pp. 2092-2099, 1993.

[49] B. M. Weckhuysen and D. E. Keller, "Chemistry, spectroscopy and the role of supported vanadium oxides in heterogeneous catalysis," *Catal. Today* , vol. 78, pp. 25-46, 2003.

[50] N. F. Dummer, J. K. Bartley and G. J. Hutchings, "Vanadium Phosphate Materials as Selective Oxidation Catalysts," *Adv. Catal.,* vol. 54, pp. 189-247, 2011.

[51] C. Wu, F. Feng and Y. Xie, "Design of vanadium oxide structures with controllable electrical properties for energy applications," *Chem. Soc. Rev.,* vol. 42, pp. 5157-5183, 2013.

[52] V. P. Prasadam, N. Bahlawane, F. Mattelaer, G. Rampelberg, C. Detavernier, L. Fang, Y. Jiang, K. Martens, I. P. Parkin and I. Papakonstantinou, "Atomic layer deposition of vanadium oxides: process and application review," *Mater. Today Chem.,* vol. 12, pp. 396-423, 2019.

[53] C. Delmas, H. Cognacauradou, J. M. Cocciantelli, M. Menetrier and J. P. Doumerc, " The LixV2O5 system - an overview of the structure modifications induced by the lithium intercalation," *Solid State Ionics,* vol. 69, pp. 257-264, 1994.

[54] E. Ostreng, K. B. Gandrud, Y. Hu, O. Nilsen and H. Fjellvag, "High power nanostructured V2O5 thin film cathodes by atomic layer deposition," *J. Mater. Chem.* , vol. 2, pp. 15044-15051, 2014.

[55] Y. Xie and C. Z. Wu, "Design of nanoarchitectured electrode materials applied in new-generation rechargeable lithium ion batteries," *Dalton T.,* p. 5235, 2007.

[56] Z. Wan, Z. Zou, J. Wang, F. Long and Y. Wu, "Synthesis and Electrochemical Properties of Flower-like Na-doped V6O13 Cathode Materials for Li-ion Batteries," *Int. J. Electrochem. Sci.* , vol. 13, pp. 6565-6576, 2018.

[57] F. Niklaus, A. Decharat, C. Jansson and G. Stemme, "Performance model for uncooled infrared bolometer arrays and performance predictions of bolometers operating at atmospheric pressure," *Infrared Phys. Technol.* , vol. 51, pp. 168-177, 2008.

[58] R. B. Darling and S. Iwanaga, "Structure, properties, and MEMS and microelectronic applications of vanadium oxides," *Sadhana* , vol. 34, pp. 531-542, 2009.

[59] M. Salimi, A. Esrafili, M. Gholami, A. J. Jafari, R. R. Kalantary, M. Farzadkia, M. Kermani and H. R. Sobhi, "Contaminants of emerging concern: a review of new approach in AOP Technologies," *Environ. Monit. Assess.,* vol. 189, p. 414, 2017.

[60] J. He, X. Yang, B. Men and D. Wang, "Interfacial mechanisms of heterogeneous Fenton reactions catalyzed by iron-based materials: A review," *J. Environ. Sci.* , vol. 39, pp. 97-109, 2016.

[61] A. Hassan, T. Iqbal, M. B. Tahir and S. Afsheen, "A review on copper vanadate-based nanostructures for photocatalysis energy production," *Int. J. Energ. Res.* , vol. 43, pp. 9-28, 2019.

[62] H. J. H. Fenton, "Oxidation of tartaric acid in the presence of iron," *J. Chem. Soc. Trans.*, vol. 65, pp. 899-910, 1894.

[63] L. Clarizia, D. Russo, I. D. Somma, R. Marotta and R. Andreozzi, "Homogeneous photo-Fenton processes at near neutral pH: A review," *Appl. Catal. B* , vol. 209, pp. 358-371, 2017.

[64] S. R. Pouran, A. R. A. Aziz and W. M. A. W. Daud, "Review on the main advances in photo-Fenton oxidation system for recalcitrant wastewaters," *J. Ind. and Eng. Chem.* , vol. 21, pp. 53-69, 2015.

[65] A. D. Bokare and W. Choi, "Review of iron-free Fenton-like systems for activating H2O2 in advanced oxidation processes," *J. Hazard. Mater.*, vol. 275, pp. 121-135, 2014.

[66] M. Zhang, Y. Niu and Y. Xu, "Heterogeneous Fenton-like magnetic nanosphere coated with vanadium oxide quantum dots for enhanced organic dyes decolorization," *J. Colloid and Interf. Sci.* , vol. 579, pp. 269-281, 2020.

[67] M. Yaqoot, P. Diwan and T. C. Kandpal, "Review of barriers to the dissemination of decentralized renewable energy systems," *Renew. Sustain. Energy Rev.*, vol. 58, pp. 477-490, 2016.

[68] J. Benedek, T. T. Sebestyen and B. Bartok, "Evaluation of renewable energy sources in peripheral areas and renewable energy-based rural development," *Renew. Sustain. Energy Rev.*, vol. 90, pp. 516-535, 2018.

[69] L. G. Arnaut, M. Barroso and C. Serpa, "Solar energy conversion," in *Applied Photochemistry*, Dordrecht, Netherlands, Springer, 2013, pp. 267-304.

[70] G. L. Chiarello and E. Selli, "Photocatalytic hydrogen production," *Recent Pat. Eng.*, vol. 4, p. 155, 2010.

[71] A. A. Ismail and D. W. Bahnemann, "Photochemical splitting of water for hydrogen production by photocatalysis: A review," *Sol. Energ. Mat. Sol. C.*, vol. 128, p. 85, 2014.

[72] M. R. Gholipour, C. T. Dinh, F. Beland and T. O. Do, "Nanocomposite hetero¬junctions as sunlight-driven photocatalysts for hydrogen production from water splitting," *Nanoscale* , vol. 7, p. 8187, 2015.

[73] A. Fujishima and K. Honda, "Electrochemical photolysis of water at a semicon¬ductor electrode," *Nature* , vol. 238, pp. 37-38, 1972.

[74] C. H. Liao, C. W. Huang and J. C. C. Wu, "Hydrogen production from semiconductor-based photocatalysis via water splitting," *Catalysts,* vol. 2, p. 490, 2012.

[75] A. O. Ibhadon and P. Fitzpatrick, "Heterogeneous photocatalysis: Recent advances and applications," *Catalysts,* vol. 3, p. 189, 2013.

[76] F. Mattelaer, K. Geryl, G. Rampelberg, T. Dobbelaere, J. Dendooven and C. Detavernier, "Atomic layer deposition of vanadium oxides for thin-film lithium-ion battery applications," *RSC Adv.*, vol. 6, pp. 114658-114665, 2006.

[77] F. Mattelaer, K. Geryl, G. Rampelberg, J. Dendooven and C. Detavernier, "Amorphous and crystalline vanadium oxides as high-energy and high-power cathodes for three-dimensional thin-film lithium ion batteries," *ACS Appl. Mater. Interfaces,* vol. 9, pp. 13121-13131, 2017.

[78] A. M. Cao, J. S. Hu, H. P. Liang and L. J. Wan, "Self-Assembled Vanadium Pentoxide (V2O5) Hollow Microspheres from Nanorods and Their Application in Lithium-Ion Batteries," *Angew. Chem. Int. Ed.*, vol. 44, p. 4391, 2005.

[79] J. Livage, "Hydrothermal Synthesis of Nanostructured Vanadium Oxides," *Materials* , vol. 3, pp. 4175-4195, 2010.

[80] D. Adler, "Mechanisms for metal-nonmetal transitions in transition-metal oxides and sulfides," *Rev. Mod. Phys.,* vol. 40, pp. 714-736, 1968.

[81] P. Yu and M. Cardona, Fundamentals of semiconductors: physics and materials properties, Heidelberg, Germany: Springer Verlag, 2010.

[82] C. Batista, R. M. Ribeiro and V. Teixeira, "Synthesis and characterization of VO2-based thermochromic thin films for energy-efficient windows," *Nanoscale Res. Lett.,* vol. 6, p. 301, 2011.

[83] S. Surnev, M. G. Ramsey and F. P. Netzer, "Vanadium oxide surface studies," *Prog. Surf. Sci.,* vol. 73, pp. 117-165, 2003.

[84] V. Eyert and K. H. Hoch, "Electronic structure of V2O5: Role of octahedral deformations," *Phys. Rev. B,* vol. 57, pp. 12727-12737, 1998.

[85] K. Hermann, A. Chakrabarti, R. Druzinic and M. Witko, "Ab initio density functional theory studies of hydrogen adsorption at the V2O5(010) surface," *Phys. Stat. Sol.* , vol. 173, pp. 195-208, 1999.

[86] M. A. Kirsanova, A. S. Akmaev, M. V. Gorbunov, D. Mikhailova and A. M. Abakumov, "Sodium-vanadium bronze Na9V14O35: An electrode material for Na-ion batteries," *Molecules* , vol. 27, no. 1, p. 86, 2022.

[87] J. C. Parker, D. J. Lam, Y. N. Xu and W. Y. Ching, "Optical properties of vanadium pentoxide determined from ellipsometry and band-structure calculations," *Phys. Rev. B,* vol. 42, pp. 5289-5293, 1990.

[88] Y. Wang, K. Takahashi, H. Shang and G. Cao, "Synthesis and Electrochemical Properties of Vanadium Pentoxide Nanotube Arrays," *J. Phys. Chem. B Lett.* , vol. 109, pp. 3085-3088, 2005.

[89] M. Alsawafta, A. Almoabadi, S. Badilescu and V. V. Truong, "Improved Electrochromic Properties of Vanadium Pentoxide Nanorods Prepared by Thermal Treatment of Sol-Gel Dip-Coated Thin Films," *J. Electrochem. Soc.* , vol. 162, pp. H466-H472, 2015.

[90] A. Talledo, A. M. Andersson and C. G. Granqvist, "Structure and optical absorption of LiyV2O5 thin films," *J. Appl. Phys.* , vol. 69, pp. 3261-3265, 1991.

[91] G. S. Nadkarni and V. S. Shirodkar, "Experiment and theory for switching in Al/V2O5/Al devices," *Thin Solid Films,* vol. 105, pp. 115-129, 1983.

[92] E. E. Chain, "Optical properties of vanadium dioxide and vanadium pentoxide thin films," *Appl. Opt.* , vol. 30, pp. 2782-2787, 1991.

[93] L. Liu, F. Cao, T. Yao, Y. Xu, M. Zhou, B. Qu, B. Pan, C. Wu, S. Wei and Y. Xie, "New-phase VO2 micro/nanostructures: investigation of phase transformation and magnetic property.," *New J. Chem.,* vol. 36, p. 619, 2012.

[94] J. Xie, C. Wu, S. Hu, J. Dai, N. Zhang, J. Feng, J. Yang and Y. Xie, "Ambient rutile VO2(R) hollow hierarchitectures with rich grain boundaries from new-state nsutite-type VO2, displaying enhanced hydrogen adsorption behavior," *Phys. Chem. Chem. Phys.*, vol. 14, p. 4810, 2012.

[95] A. Cavalleri, C. Toth, C. W. Siders, J. A. Squier, F. Raksi, P. Forget and J. C. Kieffer, "Femtosecond structural dynamics in VO2 during an ultra fast solid-solid phase transition," *Phys. Rev. Lett.* , vol. 87, p. 237401, 2001.

[96] X. Wang, H. Qi, X. Hu, Z. Yu, S. Ding, Z. Du and Q. Gong, "Advances in Photonic Devices Based on Optical Phase-Change Materials," *Molecules,* vol. 26, no. 9, p. 2813, 2021.

[97] M. Liu, H. Y. Hwang, H. Tao, A. C. Strikwerda, K. B. Fan, G. R. Keiser, A. Sternbach, K. G. West, S. Kittiwatanakul, J. W. Lu, S. A. Wolf, F. G. Omenetto, X. Zhang, K. A. Nelson and R. D. Averitt, "Terahertz-field-induced insulator-to-metal transition in vanadium dioxide metamaterial," *Nature,* vol. 487, pp. 345-348, 2012.

[98] S. Biermann, A. Poteryaev, A. I. Lichtenstein and A. Georges, "Dynamical singlets and correlation-assisted peierls transition in VO2," *Phys. Rev. Lett.*, vol. 94, p. 026404, 2005.

[99] D. Adler and H. Brooks, "Theory of semicondutor to metal transitions," *Phys. Rev.*, vol. 155, pp. 826-840, 1967.

[100] B. S. Borisov, S. T. Koretkaya, V. G. Mokerov, A. V. Rakov and S. G. Solovev, "Electrical and optical properties of VO2 near semiconductor-semimetal transition point," *Sov. Phys. – Solid State (Engl. Transl.),* vol. 12, pp. 1763-1766, 1971.

[101] J. Livage, "Optical and electrical properties of vanadium oxides synthesized from alkoxides," *Coordin. Chem. Rev.* , vol. 190, pp. 391-403, 1999.

[102] G. Xu, P. Jin, M. Tazawa and K. Yoshimura, "Thickness dependence of optical properties of VO2 thin films epitaxially grown on sapphire (0001)," *AppL. Surf. Sci.*, vol. 244, pp. 449-452, 2005.

[103] C. G. Granqvist, Handbook of inorganic electrochromic materials, Amsterdam, Netherlands: Elsevier, 1995.

[104] Z. Shao, H. Luo and P. Jin, "Recent progress in the phase-transition mechanism and modulation of vanadium dioxide materials," *NPG Asia Materials,* vol. 10, pp. 581-605, 2018.

[105] N. B. Aetukuri, N. B. Aetukuri, A. X. Gray, M. Drouard, M. Cossale, L. Gao, L. Reid, R. Kukreja, H. Ohldag, C. A. Jenkins, E. Arenholz, K. P. Roche, A. H. Durr, M. G. Samant and S. Parkin, "Control of the metal-insulator transition in vanadium dioxide by modifying orbital occupancy," *Nat. Phys.*, vol. 9, pp. 661-666, 2013.

[106] A. H. Ardakani, A. Nie, P. M. Marley, Y. Zhu, P. J. Phillips, S. Singh, M. Mashayek, G. Sambandamurthy, K. Low, R. B. Klie, S. Banerjee, G. M. Odegard and R. S. Yassar, "Atomic origins of monoclinic-tetragonal (rutile) phase transition in doped VO2 nanowires," *Nano Lett.*, vol. 15, pp. 7173-7188, 2015.

[107] M. Marezio, D. B. McWhan, J. P. Remeika and P. D. Dernier, "Structural aspects of the metal-insulator transitions in Cr-doped VO2," *Phys. Rev. B,* vol. 5, p. 2541, 1972.

[108] W. Bruckner, U. Gerlach and B. Thuss, "Phase diagram of V1-xAlxO2," *Phys. Status Solidi* , vol. 40, pp. K131-K134, 1977.

[109] R. M. Cornell and U. Schwertmann, The iron oxides: structure, properties, reactions, occurrences and uses, Weinheim, Germany: Wiley VCH, 2003.

[110] T. Saha-Dasgupta, O. K. Andersen, J. Nuss, A. I. Poteryaev, A. Georges and A. I. Lichtenstein, "Electronic structure of V2O3: Wannier orbitals from LDA-NMTO calculations.," *arXiv:0907.2841 [cond-mat.mtrl-sci],* 2009.

[111] S. Yamazaki, C. Li, K. Ohoyama, M. Nishi, M. Ichihara, H. Ueda and Y. Ueda, "Synthesis, structure and magnetic properties of V4O9 - A missing link in binary vanadium oxides," *J. Solid State Chem.*, vol. 183, pp. 1496-1500, 2010.

[112] Y. Zhang, X. Liu, G. Xie, L. Yu, S. Yi, M. Hu and C. Huang, "Hydrothermal synthesis, characterization, formation mechanism and electrochemical property of V3O7·H2O single-crystal nanobelts," *Mater. Sci. Eng. B,* vol. 175, pp. 164-171, 2010.

[113] G. S. Zakharova, V. L. Volkov, C. Taschner, I. Hellmann, A. Leonhardt, R. Klingeler and B. Buchner, "Synthesis and characterization of V3O7.H2O nanobelts," *Solid State Commun.* , vol. 149, pp. 814-817, 2009.

[114] M. Cristopher, P. Karthick, R. Sivakumar, C. Gopalakrishnan, C. Sanjeeviraja and K. Jeyadheepan, "On the preparation of Tri-vanadium hepta-oxide thin films for electrochromic applications," *Vacuum* , vol. 160, pp. 238-245, 2019.

[115] I. Mjejri and A. Rougier, "Color Switch in V3O7.H2O cycled in Li and Na based electrolytes: novel vanadium oxide based electrochromic material," *J. Mater. Chem. C,* vol. 8, pp. 3631-3638, 2020.

[116] X. Chen, S. Shen, L. Guo and S. S. Mao, "Semiconductor based photocatalytic hydrogen generation," *Chem. Rev.,* vol. 110, p. 6503, 2010.

[117] M. Mosleh, "Nanocrystalline iron vanadate: facile morphology-controlled preparation, characterization and investigation of optical and photocatalytic properties," *J. Mater. Sci.: Mater. Electron.,* vol. 28, pp. 5866-5871, 2017.

[118] M. Ghiyasiyan-Arani, M. Salavati-Niasari and S. Naseh, "Enhanced photodegradation of dye in waste water using iron vanadate nanocomposite; ultrasound-assisted preparation and characterization," *Ultrason. - Sonochem.,* vol. 39, pp. 494-503, 2017.

[119] A. Heydari, M. Sheykhan, M. Sadeghi and I. Radfar, "Nano-Rods of FeVO4: an Efficient Heterogeneous Catalyst for Chemo-Selective Oxidation of Benzylic Alcohols," *Inorganic and Nano-Metal Chemistry* , vol. 47, pp. 248-255, 2016.

[120] S. Zhang, Y. Sun, C. Li and L. Ci, "Cu3V2O8 hollow spheres in photocatalysis and primary lithium batteries," *Solid State Sci.* , vol. 25, pp. 15-21, 2013.

[121] N. Kumada, T. Takei, R. Haramoto, Y. Yonesaki, Q. Dong, N. Kinomura, S. Nishimoto, Y. Kameshima and M. Miyake, "Preparation and crystal structure of a new bismuth vanadate, Bi3.33(VO4)2O2," *Mater. Res. Bull.,* vol. 46, pp. 962-965, 2011.

[122] M. Choi, "Photocatalytic and photoelectrochemical activities of strained BiVO4," *Appl. Phys. Lett.* , vol. 118, p. 161901, 2021.

[123] J. Gan, X. Lu and Y. Tong, "Towards highly efficient photoanodes: boosting sun-light-driven semiconductor nanomaterials for water oxidation," *Nanoscale* , vol. 6, p. 7142, 2014.

[124] K. R. Tolod, S. Hernandez and N. Russo, "Recent advances in the $BiVO_4$ photo¬catalyst for sun-driven water oxidation: Top-performing photoanodes and scale-up challenges," *Catalysts,* vol. 7, p. 13, 2017.

[125] Y. Park, K. J. McDonald and K. S. Choi, "Progress in bismuth vanadate photo-anodes for use in solar water oxidation," *Chem. Soc. Rev.,* vol. 42, p. 2321, 2013.

[126] W. Y. Teoh, J. A. Scott and R. Amal, "Progress in heterogeneous photocatalysis: from classical radical chemistry to engineering nanomaterials and solar reactors," *J. Phys. Chem. Lett.,* vol. 3, pp. 629-639, 2012.

[127] T. Tachikawa, T. Ochi and Y. Kobori, "Crystal-face-dependent charge dynamics on a $BiVO_4$ photocatalyst revealed by single-particle spectroelectrochemistry," *ACS Catal.,* vol. 6, pp. 2250-2256, 2016.

[128] H. L. Tan, X. Wen, R. Amal and Z. H. Ng, "$BiVO_4$ {010} and {110} relative exposure extent: governing factor of surface charge population and photocatalytic activity," *J. Phys. Chem. Lett.,* vol. 7, pp. 1400-1405, 2016.

[129] Y. Ma, S. R. Pendlebury, A. Reynal, F. L. Formal and J. R. Durrant, "Dynamics of photogenerated holes in undoped $BiVO_4$ photoanodes for solar water oxidation," *Chem. Sci.,* vol. 5, pp. 2964-2973, 2014.

[130] J. Ravensbergen, F. F. Abdi, J. H. Santen, R. N. Frese, B. Dam, R. Krol and J. T. M. Kennis, "Unraveling the Carrier Dynamics of $BiVO_4$: A Femtosecond to Microsecond Transient Absorption Study," *J. Phys. Chem. C,* vol. 118, pp. 27793-27800, 2014.

[131] R. N. Vannier, E. Pernot, M. Anne, O. Isnard, G. Nowogrocki and G. Mairesse, "$Bi_4V_2O_{11}$ polymorph crystal structures related to their electrical properties," *Solid State Ionics,* vol. 157, pp. 147-153, 2003.

[132] G. Mairesse, P. Roussel, R. N. Vannier, M. Anne, C. Pirovano and G. Nowogrocki, "Crystal structure determination of α, β and γ-$Bi_4V_2O_{11}$ polymorphs. Part I: γ and β-$Bi_4V_2O_{11}$," *Solid State Sci.,* vol. 5, pp. 851-859, 2003.

[133] G. Mairesse, P. Roussel, R. N. Vannier, M. Anne and G. Nowogrocki, "Crystal structure determination of α, β and γ-$Bi_4V_2O_{11}$ polymorphs. Part II: crystal structure of α-$Bi_4V_2O_{11}$," *Solid State Sci.,* vol. 5, pp. 861-869, 2003.

[134] S. Lakkepally, Y. Kalegowda, V. Ramarao, E. Hanumantharayappa and A. Siddaramanna, "Room temperature synthesis of amorphous $Bi_4V_2O_{11}$ as cathode material for Li secondary batteries," *Mater. Res. Express,* vol. 5, p. 115501, 2018.

[135] M. Liang, Z. Yang, Y. Mei, H. Zhou and S. Yang, "Dye-Sensitized-Assisted, Enhanced Photocatalytic Activity of TiO_2/$Bi_4V_2O_{11}$," *Nano,* p. 1850028, 2018.

[136] T. Lehnen, M. Valldor, D. Niznansky and S. Mathur, "Hydrothermally grown porous $FeVO_4$ nanorods and their integration as active material in gas-sensing devices," *J. Mater. Chem. A* , vol. 2, p. 1862, 2014.

[137] M. G. Baeis, S. H. Mousavi and M. R. Jeddy, "Controlled synthesis and characterization of iron vanadate magnetic nanoparticles: investigation it's photodegradation of Rhodamine B," *J. Mater. Sci.: Mater. Electron.,* vol. 28, pp. 1480-1484, 2017.

[138] V. D. Nithya, R. K. Selvan, C. Sanjeeviraja, D. M. Radheep and S. Arumugam, "Synthesis and characterization of $FeVO_4$ nanoparticles," *Mater. Res. Bull.,* vol. 46, pp. 1654-1658, 2011.

[139] J. H. Deng, J. Y. Jiang, Y. Y. Zhang, X. P. Lin, C. M. Du and Y. Xiong, "$FeVO_4$ as a highly active heterogeneous Fenton-like catalyst towards the degradation of Orange II," *Appl. Catal. B,* vol. 84, pp. 468-473, 2008.

[140] B. Ozturk and G. S. P. Soylu, "Synthesis of surfactant-assisted $FeVO_4$ nanostructure: characterization and photocatalytic degradation of phenol," *J. Mol. Catal. A - Chem.* , vol. 398, pp. 65-71, 2015.

[141] M. Zhang, Y. Ma, D. Friedrich, R. Krol, L. H. Wong and F. F. Abdi, "Elucidation of opto-electronic and photoelectrochemical properties of $FeVO_4$ photoanodes for solar water oxidation," *J. Mater. Chem. A,* vol. 6, pp. 548-555, 2018.

[142] M. Arunachalam, G. Yun, K. S. Ahn and S. H. Kang, "Revealing the beneficial effects of $FeVO_4$ nanoshell layer on the $BiVO_4$ inverse opal core layer for photoelectrochemical water oxidation," *J. Phys. Chem. C,* vol. 121, pp. 7625-7634, 2017.

[143] D. P. Dutta, M. Ramakrishnan, M. Roy and A. Kumar, "Effect of transition metal doping on the photocatalytic properties of $FeVO_4$ nanoparticles," *J. Photoch. Photobio. A,* vol. 335, pp. 102-111, 2017.

[144] S. Lakkepally, Y. Kalegowda, N. Ganganagappa and A. Siddaramanna, "A new and effective approach for $Fe_2V_4O_{13}$ nanoparticles synthesis: Evaluation of electrochemical performance as cathode for lithium secondary batteries," *J. Alloy. Compd.,* vol. 737, pp. 665-671, 2018.

[145] D. Tang, A. J. E. Rettie, O. Mabayoje, B. R. Wygant, Y. Lai, Y. Liu and C. B. Mullins, "Facile Growth of Porous $Fe_2V_4O_{13}$ Films for Photoelectrochemical Water Oxidation," *J. Mater. Chem. A,* vol. 4, pp. 3034-3042, 2016.

[146] P. Li, Y. Zhou, H. Li, Q. Xu, X. Meng, X. Wang, M. Xiao and Z. Zou, "All-solid-state Z-scheme system arrays of $Fe_2V_4O_{13}$/RGO/CdS for visible light-driving photocatalytic CO_2 reduction into renewable hydrocarbon fuel," *Chem. Commun.,* vol. 51, pp. 800-803, 2015.

[147] L. F. Zhang, J. Zhou and C. Y. Zhang, "pH-controlled growth of ultrathin iron vanadium oxide (FeV_3O_8) nanoplatelets with high visible-light photo-catalytic activity," *J. Mater. Chem. A,* vol. 2, p. 14903, 2014.

[148] I. V. B. Maggay, L. M. Z. Juan, J. S. Lu, M. T. Nguyen, T. Yonezawa, T. S. Chan and W. R. Liu, "Electrochemical properties of novel FeV_2O_4 as an anode for Na-ion batteries," *Sci. Rep-UK* , vol. 8, p. 8839, 2018.

[149] H. Mandal, S. Shyamal, P. Hajra, A. Bera, D. Sariket, S. Kundu and C. Bhattacharya, "Development of ternary iron vanadium oxide semiconductors for their applications in Photoelectrochemical Water Oxidation," *RSC Adv.,* vol. 6, pp. 4992-4999, 2016.

[150] M. Ghiyasiyan-Arani, M. Masjedi-Arani and M. Salavati-Niasari, "Facile synthesis, characterization and optical properties of copper vanadate nanostructures for enhanced photocatalytic activity," *J. Mater. Sci.: Mater. Electron.,* vol. 27, pp. 4871-4878, 2016.

[151] K. Rajeshwar, M. K. Hossain, R. T. Macaluso, C. Janaky, A. Varga and P. J. Kulesza, "Review – Copper oxide-based ternary and quaternary oxides: Where solid-state chemistry meets photoelectrochemistry," *J. Electrochem. Soc.,* vol. 164, no. 4, pp. H3192-H3206, 2018.

[152] C. M. Jiang, M. Farmand, C. H. Wu, Y. S. Liu, J. Guo, W. S. Drisdell, J. K. Cooper and I. D. Sharp, "Electronic Structure, Optoelectronic Properties, and Photoelectrochemical Characteristics of γ-$Cu_3V_2O_8$ Thin Films," *Chem. Mater.,* vol. 29, pp. 3334-3345, 2017.

[153] N. T. T. Truc, N. T. Hanh, M. V. Nguyen, N. T. P. L. Chi, N. V. Noi, D. T. Tran, M. N. Ha, D. Q. Trung and T. D. Pham, "Novel direct Z-scheme $Cu_2V_2O_7$/g-C_3N_4 for visible light photocatalytic conversion of CO_2 into valuable fuels," *Appl. Surf. Sci.,* vol. 457, pp. 968-974, 2018.

[154] W. Guo, W. D. Chemelewski, O. Mabayoje, P. Xiao, Y. Zhang and C. B. Mullins, "Synthesis and Characterization of CuV_2O_6 and $Cu_2V_2O_7$: Two Photoanode Candidates for Photoelectrochemical Water Oxidation," *J. Phys. Chem. C,* vol. 119, pp. 27220-27227, 2015.

[155] T. K. Le, M. Kang and S. W. Kim, "A review on the optical characterization of V_2O_5 micro-nanostructures," *Ceram. Int.* , vol. 45, pp. 15781-15798, 2019.

[156] M. Shahid, D. S. Rhen, I. Shakir, S. P. Patole, J. B. Yoo, S. J. Yang and D. J. Kang, "Facile synthesis of single crystalline vanadium pentoxide nanowires and their photocatalytic behavior," *Mater. Lett.* , vol. 64, pp. 2458-2461, 2010.

[157] B. Liu, X. Li, Q. Zhao, J. Liu, S. Liu, S. Wang and M. O. Tade, "Insight into the Mechanism of Photocatalytic Degradation of Gaseous o-dichlorobenzene over Flower-Type V_2O_5 Hollow Spheres," *J. Mater. Chem. A,* vol. 3, pp. 15163-15170, 2015.

[158] H. Liu, Y. Gao, J. Zhou, X. Liu, Z. Chen, C. Cao, H. Luo and M. Kanehira, "Growth of oriented vanadium pentaoxide nanostructures on transparent conducting substrates and their applications in photocatalysis," *J. Solid State Chem.* , vol. 214, pp. 79-85, 2014.

[159] S. K. Jayaraj, V. Sadishkumar, T. Arun and P. Thangadurai, "Enhanced photocatalytic activity of V_2O_5 nanorods for the photodegradation of organic dyes: A detailed understanding of the mechanism and their antibacterial activity," *Mat. Sci. Semicon. Proc.,* vol. 85, pp. 112-133, 2018.

[160] M. M. Sajid, N. A. Shad, Y. Javed, S. B. Khan, Z. Zhang, N. Amin and H. Zhai, "Preparation and characterization of Vanadium pentoxide (V_2O_5) for photocatalytic degradation of monoazo and diazo dyes," *Surfaces and Interfaces,* vol. 19, p. 100502, 2020.

[161] M. Aslam, I. M. I. Ismail, N. Salah, S. Chandrasekaran, M. T. Qamar and A. Hameed, "Evaluation of Sunlight Induced Structural Changes and Their Effect on the Photocatalytic Activity of V_2O_5 for the Degradation of Phenols," *J. Hazard. Mater.,* vol. 286, pp. 127-135, 2015.

[162] N. Sahraeian, F. Esmaeilzadeh and D. Mowla, "Hydrothermal synthesis of V_2O_5 nanospheres as catalyst for hydrogen sulfide removal from sour water," *Ceram. Int.* , vol. 47, pp. 923-934, 2021.

[163] O. Monfort, T. Roch, L. Satrapinskyy, M. Gregor, T. Plecenik, A. Plecenik and G. Plesch, "Reduction of V_2O_5 thin films deposited by aqueous sol–gel method toVO_2(B) and investigation of its photocatalytic activity," *Appl. Surf. Sci.,* vol. 322, pp. 21-27, 2014.

[164] M. Saini, B. S. Dehiya and A. Umar, "VO_2(M)@CeO_2 core-shell nanospheres for thermochromic smart Windows and photocatalytic applications," *Ceram. Int.* , vol. 46, pp. 986-995, 2020.

[165] O. Monfort, T. Roch, M. Gregor, L. Satrapinskyy, T. Plecenik, A. Plecenik and G. Plesch, "Formation of vanadium oxide thin films prepared from aqueous sol-gel system," *Key Eng. Mater.,* vol. 605, pp. 79-82, 2014.

[166] Z. Chen, C. Cao, S. Chen, H. Luo and Y. Gao, "Crystallised mesoporous TiO_2(A)–VO_2(M/R) nanocomposite films with self-cleaning and excellent thermochromic properties," *Mater. Chem. A,* vol. 2, p. 11874, 2014.

[167] W. Li, S. Ji, G. Sun, Y. Ma, H. Guo and P. Jin, "Novel VO_2(M)–ZnO heterostructured dandelions with combined thermochromic and photocatalytic properties for application in smart coatings," *New J. Chem.* , vol. 40, pp. 2592-2600, 2016.

[168] X. Tao, Q. Hang, T. Wu and F. Liao, "Quasi-Hexagonal VO_2/Ag_3VO_4 Microcrystals for Photo-Catalytic Degradation of Rhodamine B," *Asian J. Chem.,* vol. 26, pp. 8291-8294, 2014.

[169] Y. Li, S. Ji, Y. Gao, H. Luo and M. Kanehira, "Core-shell VO_2@TiO_2 nanorods that combine thermochromic and photocatalytic properties for application as energy-saving smart coatings," *Sci. Rep.,* vol. 3, p. 1970, 2013.

[170] A. Z. Moshfegh and A. Ignatiev, "Photo-Enhanced Catalytic Decomposition Of Isopropanol On V205," *Catal. Lett.,* vol. 4, pp. 113-122, 1990.

[171] B. Jiang, X. Peng, Y. Qu, H. Wang, C. Tian, Q. Pan, M. Li, W. Zhou and H. Fu, "A New Combustion Route to Synthesize Mixed Valence Vanadium Oxide Heterojunction Composites as Visible-Light-Driven Photocatalysts," *ChemCatChem,* vol. 6, pp. 2553-2559, 2014.

[172] S. Zavahir, Q. Xiao, S. Sarina, J. Zhao, S. Bottle, M. Wellard, J. Jia, L. Jing, Y. Huang, J. P. Blinco, H. Wu and H. Y. Zhu, "Selective Oxidation of Aliphatic Alcohols using Molecular Oxygen at Ambient Temperature: Mixed-Valence Vanadium Oxide Photocatalysts," *ACS Catal.,* vol. 6, pp. 3580-3588, 2016.

[173] R. Arunadevi, B. Kavitha, M. Rajarajan and A. Suganthi, "Synthesis of Ce/Mo-V_4O_9 nanoparticles with superior visible light photocatalytic activity for Rhodamine-B degradation," *J. Environ. Chem. Eng.,* vol. 6, pp. 3349-3357, 2018.

[174] A. Malathi, J. Madhavan, M. Ashokkumar and P. Arunachalam, "A review on $BiVO_4$ photocatalyst: Activity enhancement methods for solar photocatalytic applications," *Appl. Catal. A,* vol. 555, pp. 47-74, 2018.

[175] M. F. R. Samsudin, S. Sufian and B. H. Hameed, "Epigrammatic progress and perspective on the photocatalytic properties of $BiVO_4$-based photocatalyst in photocatalytic water treatment technology: A review," *J. Mol. Liq.,* vol. 268, pp. 438-459, 2018.

[176] A. M. d. l. Cruz and U. M. G. Perez, "Photocatalytic properties of $BiVO_4$ prepared by the co-precipitation method:Degradation of rhodamine B and possible reaction mechanisms under visible Irradiation," *Mater. Res. Bull.,* vol. 45, pp. 135-141, 2010.

[177] F. Li, Y. Kang, M. Chen, G. Liu, W. Lv, K. Yao, P. Chen and H. Huang, "Photocatalytic degradation and removal mechanism of ibuprofen via monoclinic $BiVO_4$ under simulated solar light," *Chemosphere* , vol. 150, pp. 139-144, 2016.

[178] W. Shi, Y. Yan and X. Yan, "Microwave-assisted synthesis of nano-scale $BiVO_4$ photocatalysts and their excellent visible-light-driven photocatalytic activity for the degradation of ciprofloxacin," *Chem. Eng. J.* , Vols. 215-216, pp. 740-746, 2013.

[179] S. Kohtani, M. Koshiko, A. Kudo, K. Tokumura, Y. Ishigaki, A. Toriba, K. Hayakawa and R. Nakagaki, "Photodegradation of 4-alkylphenols using $BiVO_4$ photocatalyst under irradiation with visible light from a solar simulator," *Appl. Catal. B* , vol. 46, pp. 573-586, 2003.

[180] C. M. Huang, G. T. Pan, P. Y. Peng and T. C. K. Yang, "In situ DRIFT study of photocatalytic degradation of gaseous isopropanol over $BiVO_4$ under indoor illumination," *J. Mol. Catal. A - Chem.,* vol. 327, pp. 38-44, 2010.

[181] L. Wang, J. Liu, W. Song, H. Wang, Y. Li, J. Liu, Z. Zhao, J. Tan, Z. Duan and J. Deng, "Experimental and DFT insights of $BiVO_4$ as an effective photocatalytic catalyst for N_2O decomposition," *Chem. Eng. J.*, vol. 366, pp. 504-513, 2019.

[182] T. Saison, N. Chemin, C. Chaneac, O. Durupthy, L. Mariey, F. Mauge, V. Brezova and J. P. Jolivet, "New Insights Into $BiVO_4$ Properties as Visible Light Photocatalyst," *J. Phys. Chem. C*, vol. 119, no. 23, pp. 12967-12977, 2015.

[183] H. L. Tan, R. Amal and Y. H. Ng, "Alternative Strategies in Improving the Photocatalytic and Photoelectrochemical Activities of Visible Light-driven $BiVO_4$: A Review," *J. Mater. Chem. A*, vol. 5, pp. 16498-16521, 2017.

[184] O. Monfort, T. Roch, M. Gregor, L. Satrapinskyy, D. Raptis, P. Lianos and G. Plesch, "Photooxidative properties of various $BiVO_4/TiO_2$ layered composite films and study of their photocatalytic mechanism in pollutant degradation," *J. Environ. Chem. Eng.*, vol. 5, pp. 5143-5149, 2017.

[185] J. Li, P. Lu, W. Deng, Z. Zeng, L. Lin and G. Zhao, "Facile synthesis of sheet-like $BiVO_4/Bi_4V_2O_{11}$ composite for enhanced photocatalytic properties," *Mater. Chemi. Phys.* , vol. 254, p. 123489, 2020.

[186] Y. Pu, T. Liu, Y. Huang, C. Chen, S. I. Kim and H. J. Seo, "Optical properties and visible-light-driven photocatalytic activity of $Bi_8V_2O_{17}$ nanoparticles," *J. Nanopart. Res.*, vol. 17, p. 202, 2015.

[187] M. Ghiyasiyan-Arani, M. Salavati-Niasari, M. Masjedi-Arani and F. Mazloom, "An easy sonochemical route for synthesis, characterization and photocatalytic performance of nanosized $FeVO_4$ in the presence of aminoacids as green capping agents," *J. Mater. Sci. - Mater. El.*, vol. 29, pp. 474-485, 2018.

[188] Z. Liu, Q. Lu, M. Wei and E. Guo, "$FeVO_4$ nanobelts: controllable synthesis by electrospinning and visible-light photocatalytic properties," *J. Sol-Gel Sci. Technol.* , vol. 82, pp. 64-74, 2017.

[189] G. Tan, C. Xu, H. Ren, W. Yang, C. Zhao and A. Xia, "Synthesis and Photocatalytic Activities of Bamboo-Like $FeVO_4$ Nanocrystalline," *J. Nano Res.* , vol. 46, pp. 123-134, 2017.

[190] J. Zhang, W. Zhao, Z. Li, G. Lu and M. Zhu, "Visible-light-assisted peroxymonosulfate activation over Fe(II)/V(IV) selfdoped $FeVO_4$ nanobelts with enhanced sulfamethoxazole degradation: Performance and mechanism," *Chem. Eng. J.* , vol. 403, p. 126384, 2021.

[191] G. H. Eshaq, S. Wang, H. Sun and M. Sillanpaa, "Superior performance of $FeVO_4@CeO_2$ uniform core-shell nanostructures in heterogeneous Fenton-sonophotocatalytic degradation of 4-nitrophenol," *J. Hazard. Mater.*, vol. 382, p. 121059, 2020.

[192] R. Rahimpour, N. Chaibakhsh, M. A. Zanjanchi and Z. Moradi-Shoeili, "Fabrication of $ZnO/FeVO_4$ heterojunction nanocomposite with high catalytic activity in photo-Fenton-like process," *J. Alloy. Compd.*, vol. 817, p. 152702, 2020.

[193] M. M. Sajid, S. B. Khan, N. A. Shad, N. Amin and Z. Zhang, "Visible light assisted photocatalytic degradation of crystal violet dye and electrochemical detection of ascorbic acid using a $BiVO_4/FeVO_4$ heterojunction composite," *RSC Adv.* , vol. 8, p. 23489, 2018.

[194] Q. Wang, Z. Liu, Q. Lu, E. Guo and M. Wei, "Fabrication of Direct Z-scheme a-$Fe_2O_3/FeVO_4$ Nanobelts with Enhanced Photoelectrochemical Performance," *Chemistry Select* , vol. 3, pp. 809-815, 2018.

[195] S. Marikkani, J. V. Kumar and V. Muthuraj, "Design of novel solar-light driven sponge-like $Fe_2V_4O_{13}$ photocatalyst: A unique platform for the photoreduction of carcinogenic hexavalent chromium," *Sol. Energy*, vol. 188, pp. 849-856, 2019.

[196] K. Gowthami, B. Krishnakumar, G. Thirunarayanan, M. Swaminathan and I. Muthuvel, "Novel $Fe_2V_4O_{13}$/ZnO nano-heterojunction: Effective decomposition of methyl orange under solar light irradiation," *Mater. Today-Proc.,* vol. 29, pp. 1199-1203, 2020.

[197] Y. Y. Zhang, J. H. Deng, C. He, S. S. Huang, S. H. Tian and Y. Xiong, "Application of $Fe_2V_4O_{13}$ as a new multi-metal heterogeneous Fenton-like catalyst for the degradation of organic pollutants," *Environ. Technol.,* vol. 31, pp. 145-154, 2010.

[198] A. Nasiri and M. Nasiri, "Manganese vanadate nanostructure: facile precipitation preparation, characterization, and investigation of their photocatalyst activity," *J. Mater. Sci.: Mater. Electron.,* vol. 28, pp. 9096-9101, 2017.

[199] L. Z. Pei, N. Lin, T. Wei and H. Y. Yu, "Synthesis of manganese vanadate nanobelts and their visible light photocatalytic activity for methylene blue," *J. Exp. Nanosci.,* vol. 11, pp. 197-214, 2016.

[200] R. Wang and L. Cao, "Facile synthesis of a novel visible-light-driven $AgVO_3$/$BiVO_4$ heterojunction photocatalyst and mechanism insight," *J. Alloy. Compd.* , vol. 722, pp. 445-451, 2017.

[201] X. Cui, Z. Liu, G. Li, M. Zhang, Y. Song and J. Wang, "Self-generating $CeVO_4$ as conductive channel within CeO_2/$CeVO_4$/V_2O_5 to induce Z-scheme charge-transfer driven photocatalytic degradation coupled with hydrogen production," *Int. J. Hydrogen Energ.,* vol. 44, pp. 23921-23935, 2019.

[202] Y. Hu, J. Fan, C. Pu, H. Li, E. Liu and X. Hu, "Facile synthesis of double cone-shaped $Ag_4V_2O_7$/$BiVO_4$ nanocomposites with enhanced visible light photocatalytic activity for environmental purification," *J. Photoch. Photobio. A* , vol. 337, pp. 172-183, 2017.

[203] P. Wang, H. Yang, D. Wang, A. Chen, W. L. Dai, X. Zhao, J. Yang and X. Wang, "Activation of Kagome lattice-structured $Cu_3V_2O_7(OH)_2{\cdot}2H_2O$ volborthite via hydrothermal crystallization for boosting visible light-driven water oxidation," *Phys. Chem. Chem. Phys.,* vol. 20, pp. 24561-24569, 2018.

[204] W. Min and L. Qiong, "Synthesis and Photocatalytic Property of $Cu_3V_2O_8$ Prepared by Liquid Phase Precipitation," *Adv. Mat. Res.* , Vols. 236-238, pp. 1675-1678, 2011.

[205] S. Kalal, A. Pandey, R. Ameta and P. B. Punjabi, "Heterogeneous photo-Fenton-like catalysts $Cu_2V_2O_7$ and $Cr_2V_4O_{13}$ for an efficient removal of azo dye in water," *Cogent Chemistry,* vol. 2, p. 1143344, 2016.

[206] T. F. R. Shena, M. H. Lai, T. C. K. Yang, I. P. Fu, N. Y. Liang and W. T. Chen, "Photocatalytic production of hydrogen by vanadium oxides under visible light irradiation," *J. Taiwan Inst. of Chem. E.,* vol. 43, pp. 95-101, 2012.

[207] O. Monfort, P. Lianos and G. Plesch, "Design of Bismuth Vanadate-Based Materials: New Advanced Photoanodes for Solar Hydrogen Generation," in *Photoelectrochemical Solar Cells*, Beverly, USA, Wiley-Scrivener, 2019, pp. 219-249.

[208] Y. Wang, Z. Zhang, Z. Zhu, Z. Li, R. Vajtai, L. Ci and P. M. Ajayan, "Nanostructured VO_2 Photocatalysts for Hydrogen Production," *ACS Nano,* vol. 2, pp. 1492-1496, 2008.

[209] T. Puangpetch, S. Chavadej and T. Sreethawong, "Mesoporous-assembled V_2O_5 nanosheet synthesized via a surfactant-modified sol–gel technique and its photocatalytic H_2 production activity under visible light irradiation," *Powder Technol.,* vol. 208, pp. 37-41, 2011.

[210] J. Ran, J. Zhang, J. Yu, M. Jaroniec and S. Z. Qiao, "Earth-abundant cocatalysts for semiconductor-based photocatalytic water splitting," *Chem. Soc. Rev.,* vol. 43, p. 7787, 2014.

[211] L. Zhang, Z. Jin, X. Ma, Y. Zhang and H. Wang, "Property of iron vanadate over CdS nanorod for efficient photocatalytic hydrogen production," *New J. Chem.*, vol. 43, pp. 3609-3618, 2019.

[212] L. Zou, H. Wang and X. Wang, "High Efficient Photodegradation and photocatalytic Hydrogen Production of CdS/$BiVO_4$ Heterostructure through Z-Scheme Process," *ACS Sustainable Chem. Eng.* , vol. 5, no. 1, pp. 303-309, 2017.

[213] N. Li, X. Wu, M. Wang, K. Huang, J. He, W. Ma, H. Chen, Y. Li and S. Feng, "Facile preparation of $BiVO_4$/$FeVO_4$ heterostructure for efficient water-splitting applications," *Int. J. Hydrogen Energ.* , vol. 44, pp. 23046-23053, 2019.

[214] F. F. Abdi, L. Han, A. H. M. Smets, M. Zeman, B. Dam and R. Krol, "Efficient solar water splitting by enhanced charge separation in a bismuth vanadate-silicon tandem photoelectrode," *Nat. Commun.* , vol. 4, p. 2195, 2013.

[215] O. Monfort, L. C. Pop, S. Sfaelou, T. Plecenik, T. Roch, V. Dracopoulos, E. Stathatos, G. Plesch and P. Lianos, "Photoelectrocatalytic hydrogen produc¬tion by water splitting using $BiVO_4$ photoanodes," *Chem. Eng. J.*, vol. 286, pp. 91-97, 2016.

[216] S. J. A. Moniz, J. Zhu and J. Tang, "1D Co-Pi modified $BiVO_4$/ZnO junction cascade for efficient photoelectrochemical water cleavage," *Adv. Energy Mater.*, vol. 4, p. 1301590, 2014.

[217] G. Li, D. Zhang and J. C. Yu, "Ordered Mesoporous $BiVO_4$ through Nanocasting: A Superior Visible Light-Driven Photocatalyst," *Chem. Mater.* , vol. 20, p. 3983, 2008.

[218] O. Monfort, S. Sfaelou, L. Satrapinskyy, T. Plecenik, T. Roch, G. Plesch and P. Lianos, "Comparative study between pristine and Nb-modified $BiVO_4$ films employed for photoelectrocatalytic production of H_2 by water splitting and for photocatalytic degradation of organic pollutants under simulated solar light," *Catal. Today,* vol. 280, pp. 51-57, 2017.